Neill, I., Meliksetian, K., Allen, M. B., Navasardyan, G., and Kuiper, K. (2015) Petrogenesis of mafic collision zone magmatism: the Armenian sector of the Turkish-Iranian Plateau. *Chemical Geology*, 403, pp. 24-41.

Version: Published

http://eprints.gla.ac.uk/104390/

Deposited on: 18 May 2015

Petrogenesis of mafic collision zone magmatism: The Armenian sector of the Turkish–Iranian Plateau

Iain Neill [a,*], Khachatur Meliksetian [b], Mark B. Allen [a], Gevorg Navasardyan [b], Klaudia Kuiper [c]

[a] Department of Earth Sciences, Durham University, Science Site, DH1 3LE, Durham, UK
[b] Institute of Geological Sciences, National Academy of Sciences of Armenia, Marshal Baghramian Avenue, Yerevan 0019, Armenia
[c] Department of Earth Sciences, Vrije Universiteit Amsterdam, De Boelelaan 1085, 1081HV Amsterdam, Netherlands

ABSTRACT

The Turkish–Iranian Plateau grew after the Middle Miocene following the initial Paleogene Arabia–Eurasia collision. Authors attribute uplift to break-off of the southern Neo-Tethys slab beneath the Bitlis–Zagros Suture at ~15–10 Ma, coupled with continued plate convergence and regional crustal shortening. Since this time there has been an upsurge in mantle-derived collision magmatism over large parts of NW Iran, Eastern Anatolia and the Lesser Caucasus, potentially hundreds of kilometres from the site of southern Neo-Tethys slab break-off, >10 Myr after the proposed break-off event. Whole rock elemental and Sr–Nd–Pb–Hf isotope data are presented for <3 Ma trachy-basalt to trachy-basaltic andesite lavas erupted in Armenia in the South Caucasus. Samples formed by <5% melting of fertile subduction-modified spinel-facies lithospheric mantle, and few display elemental or isotopic evidence for contamination by the 45-km thick Mesozoic–Paleogene arc crust or South Armenian Block continental crust. Recent magmatic activity in Armenia may not be a direct consequence of southern Neo-Tethys slab break-off 300–450 km away, beneath the Bitlis Suture. Late Miocene break-off of a second (northern Neo-Tethys) slab beneath the Pontide Arc may have allowed asthenospheric upwelling over a wider area than was affected by southern Neo-Tethyan break-off. However, whole-scale delamination of mantle lithosphere is ruled out due to the modest degrees of partial melting, a lack of asthenospheric components and limited crustal involvement in magmatism. Small-scale sub-lithospheric convection may be complementary to break-off, causing localised removal of lithospheric mantle and aiding the occurrence of melting for a significant time interval after the break-off event(s). Collision magmas such as those in Armenia represent mantle-derived additions to continental crust, enriched in incompatible elements but with Th/La ratios ≤ 0.2, much lower than those calculated for continental crust (0.25–0.3). Collision magmatism in Turkic-style orogens must be balanced by infra-crustal recycling and delamination to produce bulk continental crust.

© 2015 The Authors. Published by Elsevier B.V. This is an open access article under the CC BY license (http://creativecommons.org/licenses/by/4.0/).

1. Introduction

Orogenic plateaux such as Tibet and the Bolivian Altiplano are commonly formed during continental collision and at active continental margins. This paper discusses some of the reasons why plateaux can be sites of widespread mafic magmatism derived from the melting of the asthenospheric or lithospheric mantle. Such mafic magmatism in continental collision zones is termed '*post-orogenic*' (after Turner et al., 1992) because magmatism post-dates initial collision, regional metamorphism and crustal thickening. However recent magmatism in settings such as the Turkish–Iranian and Tibetan plateaux has occurred in spite of continued overall plate convergence (e.g. Jackson et al., 1995; Williams et al., 2004). Magmatic activity is therefore not strictly post-

collisional in nature, but rather postdates initial collision. For simplicity we call such melts 'collision magmas'. When compared with mid-ocean ridges, arcs and ocean islands, the ultimate source(s) and cause(s) of partial melting to form collision magmas are enigmatic. Commonly cited triggers for collision magmatism are break-off of the subducting slab (e.g. Davies and von Blanckenburg, 1995; Keskin, 2003) and delamination or thinning of the lithospheric mantle beneath the over-riding plate (e.g. Pearce et al., 1990; Turner et al., 1992; Kay and Kay, 1993). Both processes lead to upwelling of hot asthenosphere and melting of mantle and crustal materials due to asthenospheric decompression, heating of the lower lithosphere or passage of melts through the crust. Other models include (1) melting of thickened lithosphere close to the suture between continents due to breakdown of hydrous phases (Allen et al., 2013); (2) asthenospheric convection around topographic gradients at the base of the lithosphere — i.e. 'edge-driven convection' (Missenard and Cadoux, 2012); (3) radiogenic heating within the crust (England and Thompson, 1984) and melting of deeply-subducted

* Corresponding author at: School of Geographical and Earth Sciences, University of Glasgow, Glasgow G12 8QQ, Scotland. Tel.: +44 1413 305477.
  E-mail address: iain.neill@glasgow.ac.uk (I. Neill).

continental crust (Zhao et al., 2013) and (4) small-scale lithospheric detachment (e.g., Elkins-Tanton, 2007) argued to be driven by tens to hundreds of km-wide convection cells in the upper asthenosphere (Kaislaniemi et al., 2014).

All such models for collision magmatism require testing with geophysical, geochronological and geochemical data. In this paper, we explore the elemental and isotopic geochemistry of the Pliocene–Quaternary mafic magmas of Armenia (Figs. 1, 2), part of the Turkish–Iranian Plateau in the Arabia–Eurasia collision zone, where few detailed geochemical analyses are available. Armenian collision magmatism is not clearly related to the slab break-off or whole-scale delamination models used extensively to explain Mid-Miocene-recent magmatism in Eastern Turkey (see Section 2.1). New and existing data constrain the extent of crustal interaction, the mantle source and degree of partial melting which formed the mafic Armenian magmas. This information will help judge the geodynamic process(es) responsible for magmatism. We also briefly consider the composition of these mafic collision magmas in relation to the composition of the continental crust.

2. Regional geology and geodynamics

2.1. The Turkish–Iranian Plateau and its recent magmatic record

The Turkish–Iranian Plateau (Fig. 1) covers ~1.5 × 10⁶ km² across Eastern Turkey, Iran, Armenia, Georgia and Azerbaijan. Arabia collided with this region in the Late Eocene–Oligocene (~35–25 Ma) before a proposed Middle–Late Miocene (~15–10 Ma) break-off of the north-dipping southern Neo-Tethys oceanic slab beneath the Bitlis and Zagros sutures (Keskin, 2003; Allen and Armstrong, 2008; Zor, 2008; van Hunen and Allen, 2011; McQuarrie and van Hinsbergen, 2013;

Skolbeltsyn et al., 2014). Late Oligocene to Early Miocene marine carbonates cover much of the western margin of the present plateau (Morley et al., 2009), implying that plateau growth significantly post-dates initial collision. Bottrill et al. (2012) argued that the carbonates were deposited in a dynamic basin, formed due to steepening and roll-back of the southern Neo-Tethys slab immediately before break-off. Plate convergence and compression continue today, focussed on the plateau margins in the Zagros, Greater Caucasus, Alborz and Kopeh Dagh ranges, whilst the interior of the plateau sits at ~1–2 km above sea level. Internal plateau deformation occurs typically along strike-slip fault systems, but at rates ≤2 mm/yr, such that the regional GPS-derived velocity field is not affected (Vernant et al., 2004; Allen et al., 2011; Karakhanian et al., 2013). Thrust seismicity is confined to strike-slip fault terminations, and there is no significant extension within the plateau interior (Jackson et al., 1995).

The plateau basement contains pre-Mesozoic micro-continental fragments, Mesozoic–Early Cenozoic Tethyan magmatic arc assemblages and sediments of the East Anatolian Accretionary Complex (EAAC) (e.g., Şengör, 1990). Most tectonic models for the region include a Mesozoic to Early Cenozoic north-dipping northern Neo-Tethys subduction zone beneath the Pontides in Northern Turkey and the Arc of the Lesser Caucasus in Armenia (e.g., Adamia et al., 1981; Rolland et al., 2009, 2011, 2012; Dilek et al., 2010; Sosson et al., 2010; Hässig et al., 2013; Skolbeltsyn et al., 2014). Authors have suggested that the northern Neo-Tethyan or 'Pontide' slab broke off during the Eocene (e.g., Keskin et al., 2008), but Skolbeltsyn et al. (2014) argued for a more recent (Miocene) break-off based on surface wave tomography results. This implies near-simultaneous break-off of the northern (Pontide) and southern Neo-Tethyan (Bitlis) slabs which may also have implications for collision magmatism in Eastern Anatolia and Armenia and will be discussed in Section 6.4.
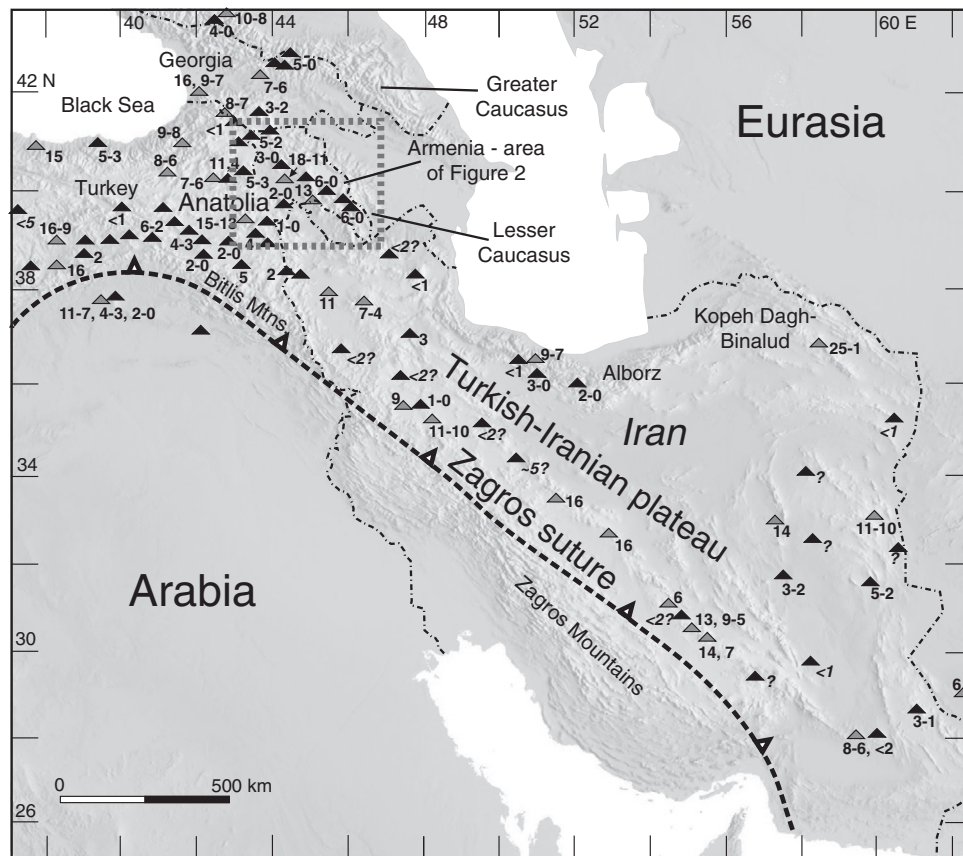

Fig. 1. Middle Miocene to Holocene magmatism of the Turkish–Iranian Plateau. Ages in Myr, with dominantly pre-Pliocene centres in grey. References and a colour version can be found in Kaislaniemi et al. (2014).
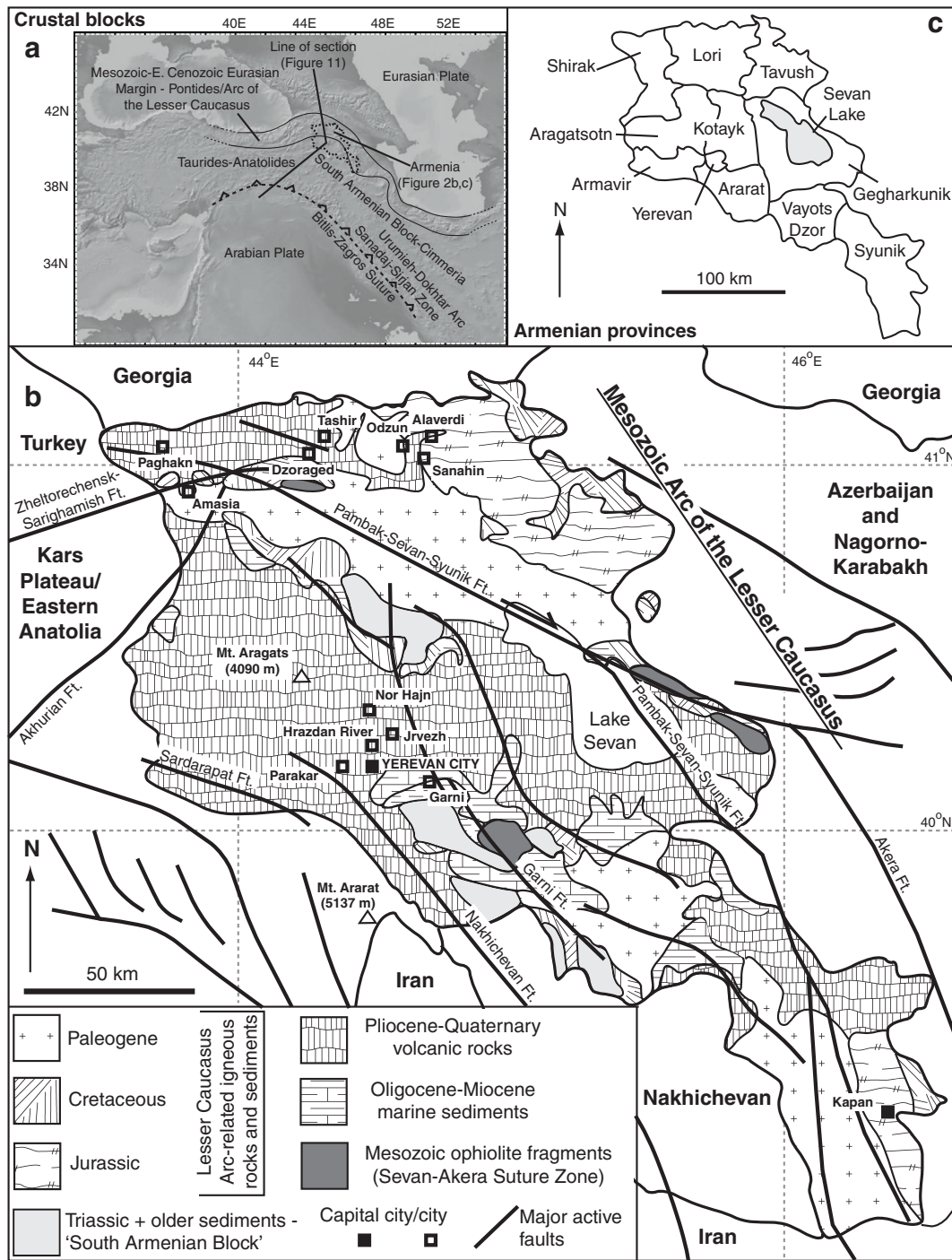
Fig. 2. a) Map of regional terranes modified from Rolland et al. (2009). b) Simplified geological map of Armenia after Kharazyan (2005) and Mederer et al. (2013) showing studied locations, with faults from Karakhanian et al. (2013). c) Armenian administrative boundaries. Note that samples from western Lori (Tashir/Dzoraged) are labelled 'S' in this work as they were collected during a sampling mission largely conducted in Shirak Province in 2011. Yerevan and Odzun/Sanahin/Alaverdi samples were collected in 2012.

Since the Middle Miocene, millions of years after the initial Arabia–Eurasia collision, mafic to felsic magmatism has become widespread (Fig. 1) (e.g., Pearce et al., 1990; Keskin, 2003; Kheirkhah et al., 2009; Dilek et al., 2010; Chiu et al., 2013; Pang et al., 2013). Southern Neo-Tethyan slab break-off and/or whole-scale lithospheric delamination models have been used to explain collision magmatism in many locations (e.g., Pearce et al., 1990; Keskin, 2003; Liotard et al., 2008; Mirnejad et al., 2010). Southern Neo-Tethys break-off beneath the Bitlis suture (Fig. 1) may be a realistic model for magmatism in NW Iran and parts of Eastern Anatolia during the Middle–Late Miocene (~15–10 Ma) (e.g. Pang et al., 2013), but it does not obviously apply to regions

overlying the ~100–225 km thick lithosphere of the Zagros Mountains (Priestley et al., 2012), or to parts of the plateau hundreds of km from the suture (Fig. 1). Magmatic activity increased during the Pliocene–Quaternary (<5 Ma) across the whole plateau (Kaislaniemi et al., 2014; Fig. 1) which is not clearly explained by Middle–Late Miocene slab break-off. Whole-scale lithospheric delamination models (e.g. Pearce et al., 1990) are also very difficult to reconcile with the Late Cenozoic magmatic record of the plateau. Removal of the sub-plateau lithospheric mantle should produce a widespread magmatic response with diachronous spatio-temporal trends related to peeling of the lithosphere (Bird, 1978). Delamination may also result in

extensive crustal melting due to contact between lower crust, hot up-welling asthenosphere, and asthenosphere-derived magmas (Babeyko et al., 2002; Best et al., 2009). However, Turkish–Iranian Plateau magmatism is temporally and spatially random in nature (see Fig. 1). Geochemical analysis indicates that many of the recent magmas, with the exception of those in the southern part of Eastern Anatolia close to the Bitlis Suture (e.g., Keskin, 2003), have experienced limited crustal interaction and are not derived from the convecting asthenosphere (Allen et al., 2013; Neill et al., 2013). Furthermore, as the plateau is not undergoing active extension, magmatism cannot be related to orogenic collapse (Jackson et al., 1995).

2.2. Geology of Armenia

Armenia lies in the Lesser Caucasus Mountains at the northern side of the Turkish–Iranian Plateau (Figs. 1,2) and is an ideal testing ground for understanding collision zone magmatism, particularly as it contains many accessible Pliocene–Quaternary volcanic centres with mafic, mantle-derived components (e.g., Neill et al., 2013). SW Armenia is underlain by the South Armenian Block, a micro-continental fragment (Şengör, 1984, 1990) consisting of Proterozoic gneisses, schists and amphibolites partially overlain by Devonian to Jurassic sediments, fragments of Jurassic and younger ophiolites and swathes of Paleogene volcanic and intrusive rocks (Şengör et al., 2008; Rolland et al., 2009) (Fig. 2b). In NE Armenia, Jurassic and Cretaceous arc rocks from the northern branch of Neo-Tethys form the so-called Arc of the Lesser Caucasus, an eastern continuation of the Pontide chain in northern Turkey (Adamia et al., 1981; 2011; Stampfli, 2000; Sosson et al., 2010; Mederer et al., 2013) (Fig. 2a,b). There are also dismembered ophiolites, forming the Sevan–Akera Suture Zone, a 400 km-long boundary between the South Armenian Block and the Arc of the Lesser Caucasus (Rolland et al., 2009; Hässig et al., 2013) (Fig. 2b). The arc-related rocks have only recently been dated using modern techniques, in the Kapan Zone in Southern Armenia (Mederer et al., 2013). These formed during two main episodes: the Middle Jurassic (~165 Ma) and the Upper Jurassic–Lower Cretaceous (~150–130 Ma) (Mederer et al., 2013). In the Upper Cretaceous, there was some magmatism which may be related to localised extension and formation of rift-like structures in a back-arc setting (Nikogosian et al., 2014). Paleogene subduction-related plutonic rocks also cut the Sevan–Akera Suture Zone (~50 Ma; Mederer et al., 2013). These may also have formed during back-arc extension related to subduction of the southern branch of Neo-Tethys, an event which also formed the Urumieh–Dokhtar Magmatic Arc in Iran (e.g. Verdel et al., 2011; Fig. 2a). A relationship to the break-off of the Pontide slab may also be possible (Keskin et al., 2008).

Northwards subduction of the southern Neo-Tethys continued south of Armenia until initial Arabia–Eurasia collision along the Bitlis–Zagros Suture during the latest Eocene to Oligocene (~35–25 Ma) (Allen and Armstrong, 2008; McQuarrie and van Hinsbergen, 2013). Magmatism re-emerged as a significant feature across the plateau after the Middle Miocene (~15–10 Ma) (Fig. 1) but did not resume until the Late Miocene (~10 Ma) in Armenia, based on K–Ar ages from Gegharkunik Province (Arutyunyan et al., 2007) (Fig. 2c). Most magmatism in Armenia is of Pliocene–Quaternary age (<3 Ma), covering >10,000 km² (Mitchell and Westaway, 1999; Karapetian et al., 2001; Lebedev et al., 2011) (Fig. 2b). Pliocene–Quaternary magmatic exposures are exclusively volcanic. Eruptive styles range from fissure-related lavas to central vent eruptions at stratovolcanoes, including Plinian eruptions and related ignimbrites (e.g., Mt. Aragats; Fig. 2) to strombolian-style eruptions at hundreds of cinder cones. These cones form large monogenetic volcanic fields and uplands. Eruption products range in composition from basalt and alkali basalt (dolerite), tephrite and basanite, to rhyolite (obsidian), with a wide range of total alkali contents (e.g. Karapetian et al., 2001; Meliksetian, 2013; Neill et al., 2013).

Extensive dolerite flows are a common variety of volcanic activity recognised across the country, filling existing topography and reaching maximum thicknesses of ~350 m — the Valley Series of Neill et al. (2013). Sheth et al. (2015) contend that these mafic flows share similar morphologies to those from much larger continental flood basalt provinces. Neill et al. (2013) used trace element and Nd–Sr isotope evidence to show that valley-filling flows and more evolved volcanic ridges and cones in Shirak Province (Fig. 2c) were co-genetic. They argued that the mafic rocks originated from melting of subduction-modified lithospheric mantle, and evolved mostly through magma mixing and fractional crystallisation. Little evidence could be discerned from Nd–Sr isotopes for crustal contamination. We return to study these mafic rocks across Armenia in greater detail than before, to judge their petrogenesis and geodynamic significance.

3. Sample age and petrography

3.1. Sampling and ages of studied samples

Previously analysed mafic Valley Series rocks from Shirak and the westernmost part of Lori Province, herein 'Shirak' (Neill et al., 2013), are augmented by whole-rock elemental analyses of 18 Pliocene–Pleistocene mafic samples from Sanahin, Odzun and Alaverdi in the east of Lori Province, and 15 mafic-intermediate Pliocene–Pleistocene samples from locations within the South Armenian Block on the Kotayk Plateau around Yerevan, including the Hrazdan River close to the city centre, at Parakar near Zvartnots Airport to the west, and around Nor Hajn and Garni to the east (Figs. 2b–c). We analysed a sub-set of samples from across the country for Sr–Nd–Pb–Hf isotopes to constrain mantle and crustal contributions to mafic magmatism along with new Pb–Hf isotope analyses of co-genetic felsic rocks from Shirak Province which had already been analysed for Nd–Sr isotopes. One Mesozoic Arc of the Lesser Caucasus sample was collected from Sanahin (Fig. 2b). Results from this sample are combined with recently-published elemental and Nd–Sr–Pb isotope data for Jurassic, Early Cretaceous and Paleogene arc rocks from near Kapan in SE Armenia (Fig. 2b) (Mederer et al., 2013). These data are used to help further discuss crustal contamination processes involved in the petrogenesis of the recent lavas.

The Pliocene–Pleistocene Valley Series mafic samples are traditionally called 'dolerite' or 'Upper Pliocene plateau basalt' lava flows in the Armenian literature, forming a stratigraphic horizon in north and central Armenia, building plateaux and filling river valleys. The Valley Series may have emanated from fissures (Shirtladze, 1958, Jrbashian et al., 1996). An Upper Pliocene age was assigned to the Valley Series when correlated with sediments containing mammalian fossils (Kharazyan, 1983). The Pliocene–Pleistocene boundary corresponds to 2.58 Ma (Cohen et al., 2013), so as these flows are mostly considered to be ≤2.5 Myr old (see below), they are of Lower Pleistocene age. Felsic volcanic ashes related to the Ridge Series (Neill et al., 2013) of the Javakheti Ridge in Shirak Province (Fig. 2c) have zircon U–Pb ion probe ages of 1.94–1.75 Ma (Presnyakov et al., 2012). The Ridge Series overlies, and is genetically related to the mafic samples of the Valley Series from Shirak and Lori (Fig. 2c), confirming an age of ≥2 Ma for the Valley Series (Neill et al., 2013). U–Pb results are corroborated by two new groundmass Ar–Ar ages of 1.84–1.80 Ma from felsic samples on the Javakheti Ridge (Karakhanian et al., unpublished data). There is a K–Ar groundmass age from a dolerite of the Akhurian river basin in Shirak of 2.5 ± 0.2 Ma (Chernyshev et al., 2002). Similar valley-filling flows in Southern Georgia are also dated using K–Ar methods to a range of 3–2 Ma (Lebedev et al., 2008a, 2008b), confirming earlier assumptions from geological and palaeontological data (Shirtladze, 1958, Kharazyan, 1983). There is a switch in magnetic polarity between the lower and upper part of the Valley Series flow sequences, although several switches occurred during the Lower Pleistocene (Kharazyan and Shirinyan, 1981 and references therein; Cohen et al., 2013).

A K–Ar age of 2.47 ± 0.17 Ma was reported for doleritic flows from a cross-section of the Hrazdan River canyon in Yerevan (Balog et al., 1990;

Fig. 2b). The sample should correspond to Y2.1 in our collection. Given an absence of weathering surfaces between flows, we assume that the Yerevan dolerites were emplaced in a short time period. An Ar–Ar groundmass age of 2.37 ± 0.03 Ma was obtained from a dolerite in a quarry at Parakar near Zvartnots Airport, corresponding to Y9.1 in this study. This age, originally obtained for an archaeological survey, has not hitherto been reported. Analytical details are reproduced in full in Supplementary Items A1 and A2. Samples from around Nor Hajn and Jrvezh near the valley of the Hrazdan River are also assumed to be of Lower Pleistocene age. Two younger flows were also sampled. A columnar-jointed flow (Y1.1), again in the Hrazdan river canyon in Ye-revan, is dated to ~150–160 Ka (Upper Pleistocene) on the basis of ar-chaeological results (Karapetyan, 1983). Columnar jointed basaltic trachy-andesites of the Azat river (Garni; Fig. 2b; Y10.1) have not been dated absolutely, but the geological map of Armenia (Kharazyan, 2005) indicates a Middle Pleistocene age (0.78–0.128 Ma). Andesitic flows overlying the Garni basaltic trachy-andesites have K–Ar ages of 0.166 ± 0.037 and 0.171 ± 0.030 Ma (Balog et al., 1990), providing a minimum age for Y10.1.

3.2. Petrography

Mafic samples from Shirak and Lori Provinces (Fig. 2c) are vesicular sub-ophitic dolerites with rare clinopyroxene and optically zoned plagioclase phenocrysts, set in a groundmass of 1–2 mm grain size, consisting of equal proportions of clinopyroxene and plagioclase and ~2% oxides. Low-pressure evolution of the magmas is indicated by the rimming or replacement of clinopyroxene by red–brown amphibole. Rarely there is interstitial quartz present. Occasional rounded quartz blebs were taken by Neill et al. (2013) to indicate mixing processes be-tween mafic and felsic end members. Some samples contain sub-mm iddingsite entirely replacing olivine, as well as a few rounded olivine crystals of <0.5 mm in diameter in some of the freshest least-evolved samples. Samples from near Yerevan (Fig. 2b) have a wider composi-tional range than the other rocks (4–9 wt.% MgO), and accordingly have more variable proportions of clinopyroxene and plagioclase. The least evolved sample, Y8.1 from Jrvezh to the east of Yerevan City, contains 2–3 mm olivine phenocrysts and glomerocrysts composed of olivine and clinopyroxene. Other samples contain only a few rounded olivine crystals and are texturally similar to, although occasionally finer-grained than the Lori and Shirak lavas. There is little difference in petrography between the Lower and Upper Pleistocene samples.

4. Analytical methods

Altered patches were removed during fly pressing and samples were then powdered by agate ball mill at Durham University. Major elements were analysed from fused glass beads using a PANalytical Axios Advanced X-ray Fluorescence (XRF) spectrometer at the University of Leicester. Powders were dissolved using standard HF–HNO$_3$ digestion techniques (Ottley et al., 2003) and solutions were run for trace ele-ments on a Thermo X2 inductively-coupled plasma mass spectrometer (ICP-MS) at the Durham Geochemistry Centre. Data quality was moni-tored using blanks, multi-run and within-run duplicates, Re–Rh spikes and five reference standards. Standard W2 (n = 23) gave first relative standard deviations of 10% or better for all transition metals (11% for Cr), the large ion lithophile elements (LILEs), high field strength ele-ments (HFSEs) and the rare earth elements (REEs). Results for samples which also underwent isotopic analysis are in Table 1, with full results and standards in Supplementary Item B.

Radiogenic isotope preparation and analysis was undertaken at the Durham Geochemistry Centre. Samples were dissolved using HF–HNO$_3$ digestion followed by elemental pre-concentration based on Dowall et al. (2007). Sample solutions were run through 1 ml pipette tips containing dilute Sr-spec resin to collect the Sr- and Pb-bearing fractions. The high field strength element (HFSE)- and Rare Earth

Element (REE)-bearing fractions were run through 10 ml polypropylene columns containing Bio-Rad AG50W-X8 200–400 mesh cation-exchange resin. Neodymium was collected as part of a general REE frac-tion. The HFSE-bearing fraction was then run through a 10 ml polypro-pylene column containing Bio-Rad AG1-X8 anion-exchange resin to separate Hf from Ti. Samples were taken up in 400–500 μl of 3% HNO$_3$.

A Thermo Neptune Multi-Collector ICP-MS was used for isotopic analysis. Sr concentrations were tested using ^{84}Sr before dilution to produce an ^{88}Sr beam of ~20 V. International reference standard NBS987 gave a mean ^{87}Sr/^{86}Sr of 0.710279 ± 0.000019 (2σ, n = 12, uncertainty = 27.2 ppm). All results, including those previously report-ed un-normalised by Neill et al. (2013), were normalised to a preferred value of 0.710240. Nd was run with J&M and Sm-doped J&M standards giving a mean ^{143}Nd/^{144}Nd of 0.511106 ± 0.000014 (2σ, n = 19, uncertainty = 26.9 ppm). Results were normalised to a preferred value of 0.511110. Hf was run with standard JMC475 giving a mean ^{176}Hf/^{177}Hf of 0.282157 ± 0.000010 (2σ, n = 9, uncertainty = 36.9 ppm). Results were normalised to a preferred value of 0.282160. Pb samples were spiked with a Tl solution to produce a Pb/Tl ratio of ~12 to minimise overlap of tails of ^{205}Tl onto ^{204}Pb and ^{206}Pb onto ^{205}Tl. Pb was run using standard NBS981 and results were corrected offline for mass bias using the ^{205}Tl/^{203}Tl ratio of the Tl spike. A ^{205}Tl/^{203}Tl ratio of 2.388770 was used to correct Pb isotope ratios. This value was changed iteratively to bring the average of Pb isotope ratios of the standard for that session as close as possible to the preferred values of Galer (1997) for NBS981. Final corrected values and errors for NBS981 were: ^{206}Pb/^{204}Pb = 16.94044 ± 0.00082; ^{207}Pb/^{204}Pb = 15.49757 ± 0.00120 and ^{208}Pb/^{204}Pb = 36.71486 ± 0.00376 (2σ, n = 10). Isotope results for mafic samples are presented in Table 2. The dataset for intermediate and felsic cinder cone and ridge-forming lava flow samples from Shirak Province is in Supplementary Item C.

5. Whole-rock geochemical results

5.1. Major elements

The majority of samples from Shirak and Lori are alkaline trachy-basalts with 49–54 wt.% SiO$_2$ (Table 1). They display some overlap into the alkali basalt and trachy-basaltic andesite fields shown in Fig. 3a. The lavas from the Yerevan region have a wider SiO$_2$ range (50–56 wt.%) and include trachy-basalts but more commonly trachy-basaltic andesites (Fig. 3a). The samples are clearly not primary magmas, with Shirak samples ranging from 4 to 7 wt.% MgO, Lori from 5 to 7 wt.%, and Yerevan from 4 to 9 wt.% (Table 1, Fig. 4a, Supplementary Item B). All of the samples are Na-rich although there is a wide range of Na$_2$O/K$_2$O ratios from 1.8 to 4.5. The lavas from Shirak and Lori fall into the medium-K field, whereas the Yerevan samples are classified as high-K to shoshonitic rocks on Fig. 3b.

5.2. Trace elements

Transition metal abundances are lower than primary basaltic assem-blages. Sc ranges from 13 to 23 ppm, Ni from 10 to 250 ppm (typically ~100 ppm) and Cr from 12 to 400 ppm (typically ~140 ppm), with the greatest variation occurring in the samples from Yerevan (Table 1 and Supplementary Item B). Samples from Shirak and Lori have modest concentrations of large ion lithophile elements (LILEs) — around 500 ppm Sr and 300–400 ppm Ba, whilst those from Yerevan range from 600 to 1200 ppm Sr and 300 to 1100 ppm Ba with the highest values in the least evolved sample, Y8.1 (Fig. 4b, Table 1, Supplementary Item B). The Shirak and Lori samples have almost identical REE profiles to one another. They are moderately LREE-enriched (La ~90–120 times chondritic values), with flat HREE patterns and very small negative Eu anomalies (Figs. 5a,b). Samples from the Yerevan area have a wider spread in REE concentrations and steeper LREE/HREE slopes compared to Shirak and Lori, albeit still with flat HREE patterns (Fig. 5c). La

Table 1

Selected elemental compositions of Late Pliocene–Early Pleistocene mafic "Valley Series" dolerites from across Armenia, for which isotopic data has also been obtained. LOI = loss-on-ignition, * = low total, b.d. = below detection. Full data can be found in Supplementary Item B. Majors in wt.%, traces in ppm. Samples S14.4, S14.5, S28.1 and S29.1 were flows probably derived from the Javakheti Ridge in Shirak Province, although these samples were picked up on the Lori side of the Lori–Shirak border. They were labelled 'S' to distinguish those from separate flows further east in Lori.

	S14.4	S29.1	S28.1	S26.2	S19.1	S14.5	L8.7	L8.3	L8.5	L8.9	L8.1	Y2.3	Y9.1	Y7.1	Y8.1	Y5.1	L3.2
Location	Dzoraged	Tashir	Tashir	Amasia	Paghakn	Dzoraged	Alaverdi	Alaverdi	Alaverdi	Alaverdi	Alaverdi	Hrazdan	Parakar	NorHajn	Jrvezh	NorHajn	Sanahin
	Shirak	Shirak	Shirak	Shirak	Shirak	Shirak	Lori	Lori	Lori	Lori	Lori	Yerevan	Yerevan	Yerevan	Yerevan	Yerevan	Lori
Easting	44.14870	44.33953	44.30911	43.76150	43.65789	44.94814	44.68623	44.68811	44.68711	44.68518	44.68844	44.49801	44.38585	44.64570	44.61396	44.59020	44.70564
Northing	41.04076	41.05486	41.08022	40.91202	41.06581	41.04071	41.09473	41.09501	41.09471	41.09441	41.09541	40.18672	40.17216	40.25031	40.18738	40.30667	41.08709
Est. age	2–3 Ma	2–3 Ma	2–3 Ma	2–3 Ma	2–3 Ma	2–3 Ma	2–3 Ma	2–3 Ma	2–3 Ma	2–3 Ma	2–3 Ma	2.5 Ma	2.4 Ma	2.5 Ma	2.5 Ma	2.5 Ma	~150 Ma
Type	Valley-filling flows																Basement
SiO_2	50.68	51.03	51.45	52.24	52.33	53.21	50.58	50.61	51.02	51.05	52.37	50.27	50.63	51.04	51.69	51.77	67.15
TiO_2	1.52	1.56	1.51	1.71	1.40	1.25	1.50	1.61	1.52	1.48	1.33	1.60	1.61	1.34	1.02	1.73	0.38
Al_2O_3	16.59	16.91	16.92	16.96	16.96	16.59	16.59	16.80	16.56	16.42	16.70	17.25	17.31	16.55	14.55	17.01	10.67
$Fe_2O_3(t)$	10.20	10.52	10.16	10.43	9.27	9.03	9.80	10.43	9.68	9.54	9.22	10.13	10.14	9.41	8.04	9.35	4.49
MgO	6.61	5.75	5.83	4.72	5.98	5.94	6.75	5.42	6.33	6.55	5.77	6.08	6.01	6.06	8.80	3.70	0.84
MnO	0.16	0.17	0.18	0.16	0.15	0.15	0.15	0.15	0.15	0.15	0.14	0.15	0.15	0.16	0.13	0.15	0.07
CaO	9.09	9.00	8.87	8.40	8.75	8.37	9.07	8.64	8.89	8.68	8.48	8.98	8.87	9.10	9.20	7.33	1.85
Na_2O	3.79	4.01	4.06	4.34	4.18	3.96	3.97	4.15	4.10	4.11	4.09	4.15	4.09	3.88	3.64	5.04	2.92
K_2O	1.09	1.18	1.20	1.19	1.19	1.48	0.97	1.10	1.09	1.20	1.30	0.99	1.00	1.31	2.07	2.15	0.88
P_2O_5	0.43	0.40	0.44	0.46	0.44	0.48	0.37	0.42	0.40	0.45	0.43	0.39	0.39	0.39	0.67	0.74	0.06
LOI	0.73	−0.14	0.05	−0.09	−0.14	−0.30	−0.31	0.47	−0.02	0.14	−0.15	−0.08	−0.54	0.60	0.08	−0.13	3.16
Total	100.89	100.40	100.67	100.56	100.52	100.16	99.76	99.93	99.75	99.77	99.68	100.03	99.66	99.84	99.88	98.83	92.48*
Mg#	56	52	53	48	56	57	55	48	54	55	53	52	51	53	66	41	25
Sc	16	22	22	22	19	23	22	21	20	21	19	22	21	19	19	19	b.d.
V	167	184	185	188	164	179	159	183	154	158	155	164	158	161	159	213	b.d.
Cr	154	129	153	131	161	162	137	138	129	142	118	132	119	155	401	11	b.d.
Co	38	42	41	35	37	33	43	38	43	38	33	37	35	37	35	25	b.d.
Ni	107	102	106	65	114	114	107	97	107	99	86	70	63	127	247	10	b.d.
Cu	46	48	44	35	40	44	44	76	88	49	67	45	43	40	57	28	b.d.
Rb	16.7	21.0	21.4	17.9	14.1	22.5	9.9	17.2	13.8	15.6	19.3	16.1	16.2	19.6	42.4	26.3	18.8
Sr	718	566	640	555	617	671	546	504	527	525	594	603	603	595	1205	967	77
Y	30.5	30.4	30.3	31.7	27.6	27.1	28.8	30.5	29.2	29.7	27.2	29.9	31.0	26.2	22.1	32.5	45.9
Zr	196	198	195	209	182	181	178	195	169	174	186	186	190	164	137	211	137
Nb	14.3	13.4	14.2	12.7	14.0	15.6	11.8	12.6	12.9	15.4	15.7	12.2	12.5	14.7	19.0	21.6	5.2
Ba	329	312	334	288	356	452	279	279	288	319	390	295	307	509	1096	787	100
Hf	3.9	3.9	3.8	4.3	3.9	4.0	4.0	4.1	4.0	3.9	3.9	4.0	4.1	3.6	3.1	4.7	4.0
Ta	0.7	0.7	0.7	0.7	0.8	0.8	0.7	0.7	0.7	0.8	0.7	0.6	0.7	0.7	0.8	1.0	0.3
Pb	4.6	4.7	4.6	4.3	5.5	6.6	4.1	7.9	4.9	5.9	6.0	4.0	4.1	5.0	8.6	9.0	1.9
Th	2.2	2.6	2.6	2.8	3.1	3.8	2.3	2.6	2.6	2.8	3.7	2.3	2.4	3.5	6.7	4.3	2.6
U	0.7	0.6	0.8	0.3	0.3	0.9	0.6	0.4	0.5	1.0	0.8	0.7	0.5	0.6	1.4	0.6	0.9
La	23	20	24	21	28	35	22	23	24	26	31	24	24	30	53	58	12
Ce	46	42	47	43	51	66	44	45	47	51	56	48	48	57	99	109	27
Pr	5.2	6.0	6.6	6.3	6.9	8.5	5.9	6.0	6.2	6.7	6.9	6.5	6.7	7.4	12.9	13.9	4.1
Nd	24.7	23.9	26.0	25.1	26.8	31.3	23.9	24.6	25.0	26.5	26.2	26.0	27.4	27.7	46.7	51.3	18.6
Sm	5.3	5.2	5.4	5.4	5.3	5.9	5.1	5.3	5.3	5.4	5.1	5.6	5.8	5.4	7.6	8.7	5.1
Eu	1.7	1.7	1.7	1.7	1.7	1.7	1.7	1.7	1.7	1.7	1.6	1.8	1.9	1.7	2.0	2.4	1.1
Gd	5.6	5.7	5.7	5.9	5.6	5.8	5.3	5.6	5.4	5.6	5.1	6.1	6.3	5.7	6.8	8.3	5.8
Tb	0.8	0.9	0.9	0.9	0.9	0.9	0.8	0.8	0.8	0.8	0.7	0.9	0.9	0.8	0.8	1.1	1.1
Dy	4.9	5.1	5.0	5.3	4.9	4.9	4.9	5.1	5.0	5.0	4.5	5.4	5.4	4.7	4.2	5.9	7.1
Ho	1.0	1.0	1.0	1.1	1.0	1.0	1.0	1.0	1.0	1.0	0.9	1.1	1.1	0.9	0.8	1.1	1.6
Er	2.7	2.8	2.7	2.9	2.7	2.7	2.7	2.8	2.7	2.7	2.5	2.9	3.0	2.5	2.0	3.1	4.5
Tm	0.4	0.5	0.4	0.5	0.4	0.4	0.4	0.5	0.4	0.4	0.4	0.5	0.5	0.4	0.3	0.5	0.8
Yb	2.7	2.8	2.7	2.9	2.7	2.6	2.7	2.8	2.7	2.7	2.4	2.8	3.0	2.4	1.9	2.9	4.9
Lu	0.4	0.5	0.4	0.5	0.4	0.4	0.4	0.5	0.4	0.4	0.4	0.5	0.5	0.4	0.3	0.5	0.8

Table 2

Radiogenic isotope results for Armenian Pliocene–Quaternary mafic–intermediate lavas, plus Mesozoic arc basement. Epsilon values are calculated for the present day using $(^{143}Nd/^{144}Nd)_{CHUR} = 0.512638$ and $^{176}Hf/^{177}Hf = 0.282772$ for chondritic Earth. Additional Pb and Hf isotope data plus previously published Nd and Sr isotope data for felsic samples from Shirak are in Supplementary Item C.

	$^{87}Sr/^{86}Sr$	$\pm 2\sigma$	$^{143}Nd/^{144}Nd$	$\pm 2\sigma$	εNd	$^{176}Hf/^{177}Hf$	$\pm 2\sigma$	εHf	$^{206}Pb/^{204}Pb$	$\pm 2\sigma$	$^{207}Pb/^{204}Pb$	$\pm 2\sigma$	$^{208}Pb/^{204}Pb$	$\pm 2\sigma$
Shirak, NW Armenia														
S14.4	0.704775	16	0.512859	10	+4.27	not analysed								
S14.5	0.704326	9	0.512831	4	+3.76	0.283043	6	+9.58	18.9922	15	15.6272	16	38.9939	54
S19.1	0.704165	7	0.512864	5	+4.41	0.283054	3	+9.97	18.9175	13	15.6225	12	38.9030	31
S26.2	0.704134	8	0.512862	6	+4.37	0.283041	3	+9.51	18.9696	11	15.6246	13	38.9549	33
S28.1	0.704206	8	0.512845	5	+4.04	0.283040	2	+9.47	19.0135	23	15.6287	22	38.9850	64
S29.1	0.704145	7	0.512857	5	+4.27	0.283035	2	+9.29	19.0476	15	15.6311	13	39.0087	33
Lori, NE Armenia														
L8.1	0.704258	22	0.512871	16	+4.54	not analysed			19.0112	11	15.6271	11	38.9934	30
L8.3	0.704135	22	0.512905	9	+5.21	not analysed			18.7046	13	15.6146	13	38.7058	34
L8.5	0.704136	26	0.512877	8	+4.66	0.283041	2	+9.52	18.9354	11	15.6251	11	38.9136	27
L8.7	0.704163	22	0.512884	8	+4.80	0.283051	3	+9.86	19.0079	13	15.6302	14	38.9842	38
L8.9	0.704197	20	0.512874	16	+4.60	0.283055	3	+10.00	18.9484	12	15.6248	12	38.9213	34
Yerevan area														
Y2.3	0.704080	24	0.512882	8	+4.76	0.283052	3	+9.90	19.0247	17	15.6172	20	38.9854	60
Y5.1	0.704246	16	0.512845	10	+4.03	0.283030	4	+9.12	18.9248	10	15.6126	11	38.9288	27
Y7.1	0.704346	22	0.512864	13	+4.41	0.283046	2	+9.68	19.1182	11	15.6325	12	39.0875	34
Y8.1	0.704768	10	0.512807	8	+3.29	0.283018	2	+8.69	19.1137	11	15.6521	12	39.1446	34
Y9.1	0.704044	24	0.512886	8	+4.83	0.283050	2	+9.82	19.0396	13	15.6180	12	39.0046	40
Lori basement (~150 Ma)														
L3.2	0.708058	22	0.512869	10	+4.50	0.283084	4	+11.03	19.1633	26	15.6516	28	39.1716	82

concentrations range from ~100 to 280 times chondritic values, with La/Yb$_{CN}$ of 6–21, compared to a range of 4–9 in Shirak and Lori. On Primitive Mantle-normalised trace element plots (Figs. 6a–c), samples have positive spikes for the LILEs Ba, Sr and Th, as well as LREE enrichment. Of the high field strength elements (HFSEs), Nb, Ta and Ti show prominent negative anomalies whilst Zr always has a positive anomaly compared with the surrounding REE. Zr/Hf ratios are considerably higher than the chondritic value of ~34.3 (Münker et al., 2003), ranging from 43 to 51, with the lowest values in Lori and mostly higher values elsewhere.

5.3. Radiogenic isotopes

The Lower Pleistocene mafic samples show a limited range of isotopic composition (Fig. 7a–e; Table 2). Average values expressed to two standard deviations are: $^{87}Sr/^{86}Sr$ = 0.7042 ± 0.0003; εNd = +4.40 ± 0.95; εHf = +9.57 ± 0.75; $^{206}Pb/^{204}Pb$ = 18.98 ± 0.20; $^{207}Pb/^{204}Pb$ = 15.63 ± 0.02; and $^{208}Pb/^{204}Pb$ = 38.97 ± 0.19 (Table 2). The two Upper Pleistocene samples from Yerevan were not analysed isotopically. In Sr–Nd isotope space the samples mostly lie

within the mantle array and are more depleted than Bulk Earth (Fig. 7a), similar to other mafic samples from across the northern part of the Turkish–Iranian Plateau, in particular some of Eastern Anatolia (Mount Ararat), and Georgia. A few samples have slightly higher $^{87}Sr/^{86}Sr$ and lower $^{143}Nd/^{144}Nd$ compared with the others, similar to the Paleogene and Mesozoic arc rocks in the region (see Section 6.1 for discussion). In Nd–Hf space, samples lie above the terrestrial array (Fig. 7b). Few other whole-rock Hf isotope analyses exist for the Turkish–Iranian Plateau, but it appears that the Armenian samples are the most radiogenic of those analysed for Nd–Hf isotopes so far. Shoshonites from the Eslamy Peninsula in Iran (Pang et al., 2013) lie close to the terrestrial array as shown in Fig. 7b but are less radiogenic than Bulk Earth so they are likely to have been contaminated by continental crust. Asthenosphere-derived alkali basalts from near Quchan in NE Iran lie on the terrestrial array (Kheirkhah et al., in press). Finally, small-degree melts of the mantle lithosphere from Mahabad in NW Iran (Kheirkhah et al., 2013) have been additionally analysed for Hf isotopes (Neill et al., 2013). These samples lie close to the terrestrial array, but like the Eslamy shoshonites are less radiogenic than the Armenian rocks.
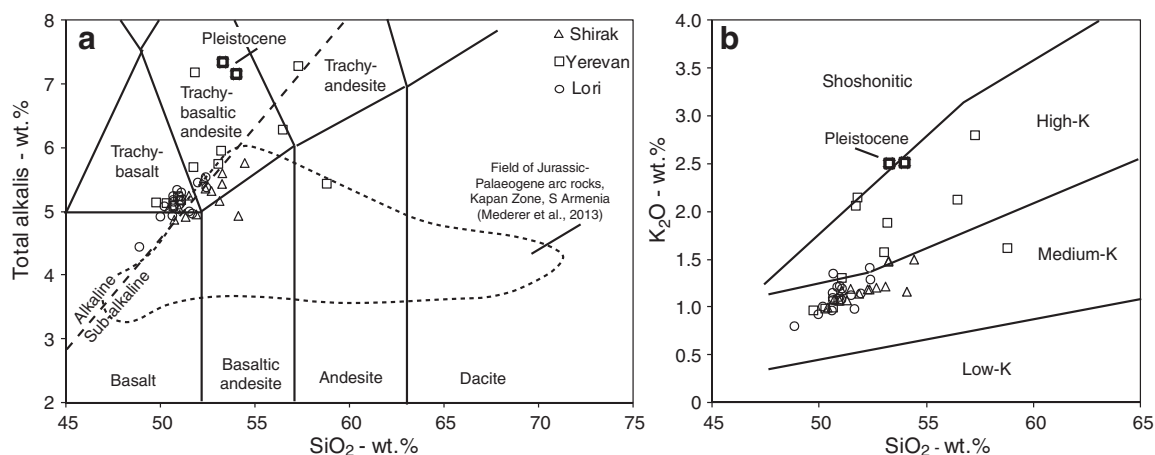

Fig. 3. a) Total alkali vs. SiO$_2$ classification diagram for studied samples (Le Bas et al., 1986). Alkaline/sub-alkaline boundary after Miyashiro (1978). b) K$_2$O vs. SiO$_2$ classification diagram after Peccerillo and Taylor (1976).
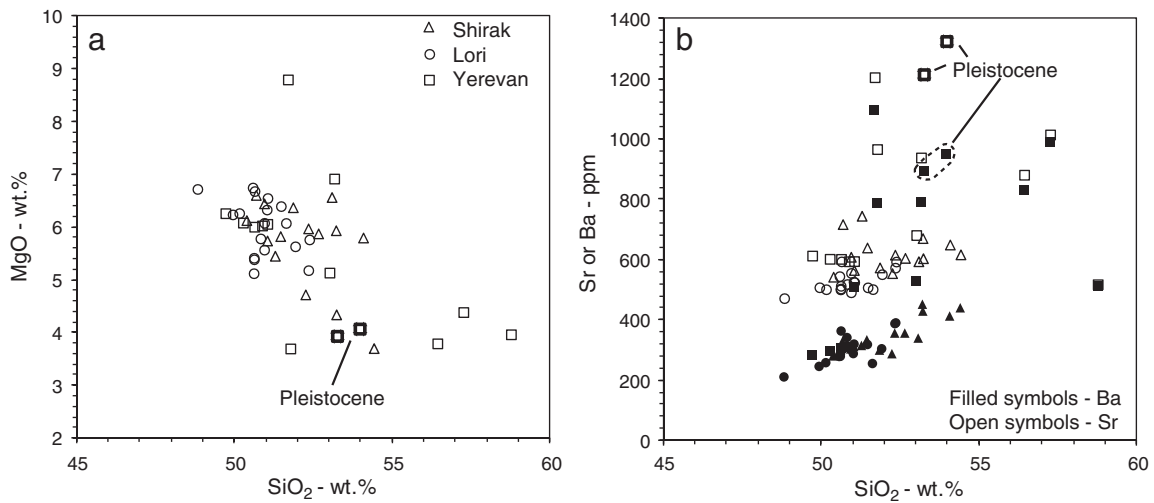
Fig. 4. a) MgO vs. SiO$_2$ Harker plot for Armenian mafic collision magmas. b) Sr and Ba concentrations in the Armenian collision magmas.
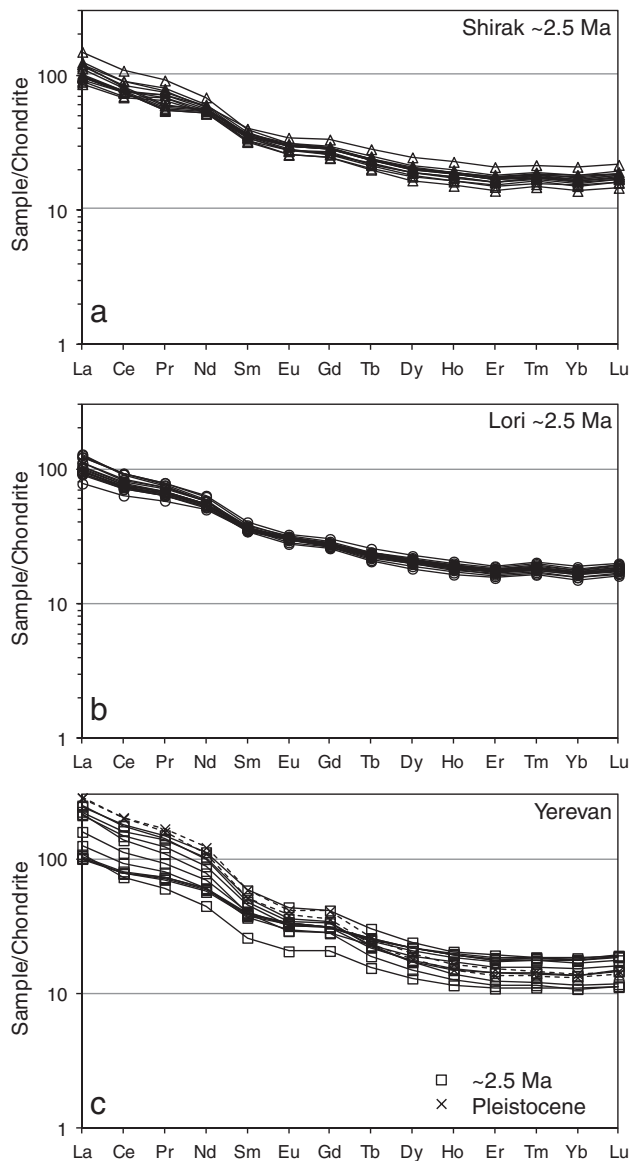

Fig. 5. a–c) Chondrite-normalised REE patterns for the studied samples (normalising values from McDonough and Sun, 1995).

On Pb isotope plots (Fig. 7c–d), the Armenian samples lie above the Northern Hemisphere Reference Line (NHRL) close to the EMII end member, at the upper end of the Indian MORB field. The samples have only slightly lower $^{208}Pb/^{206}Pb$ than EMII but cannot be directly related to an EMII source as they have much lower $^{87}Sr/^{86}Sr$ and do not form trends in isotope space pointing towards this mantle end member (Figs. 7a–b). Overall, the Armenian collision zone lavas show some variation in Pb isotope space sub-parallel to the NHRL (Fig. 7c–d; see Section 6.1 for discussion).

Many of the Mesozoic–Paleogene arc-related samples from the Kapan Zone have very similar Nd–Sr isotope systematics to the recent mafic lavas, but the Jurassic–Cretaceous samples trend towards a high $^{87}Sr/^{86}Sr$ end member (Mederer et al., 2013; Fig. 7a). There is no complementary decrease in less fluid-mobile $^{143}Nd/^{144}Nd$, which may indicate that these Mesozoic samples have experienced seawater alteration. The two Paleogene samples of Mederer et al. (2013) have lower $^{143}Nd/^{144}Nd$ ratios than the other arc rocks. Of the Mesozoic to Paleogene arc rocks, only our Mesozoic Lori sample (L3.2) was analysed for its $^{176}Hf/^{177}Hf$ ratio. This sample has very slightly higher εHf and similar εNd compared to the recent lavas (Fig. 7b). In Pb isotope space the Mesozoic–Paleogene and recent rocks differ from one another and the older rocks are displaced to lower $^{206}Pb/^{204}Pb$ compared to the recent lavas, with the exception of a single Lower Pleistocene sample from Lori which may have experienced crustal contamination and has the lowest Pb isotope ratios of all analysed Late Cenozoic samples (Fig. 7c–d). Pre-Late Cenozoic volcanic rocks lie in three groups in Pb isotope space, with slightly higher $^{206}Pb/^{204}Pb$ in the Jurassic and Paleogene rocks compared to the Late Jurassic–Early Cretaceous samples. Mederer et al. (2013) related this variation to a higher proportion of recycled continental sediment in the Jurassic and Paleogene samples.

6. Discussion

6.1. Crustal contamination of Armenian collision magmas

6.1.1. Contamination in the mafic samples

Crustal contamination in the Pleistocene mafic samples is difficult to identify using Sr and Nd isotope ratios because much of the northeastern Armenian crust contains Mesozoic and Paleogene arc rocks with depleted Nd–Sr isotope characteristics similar to those of the recent lavas (Mederer et al., 2013; Neill et al., 2013). The isotopic composition of the South Armenian Block is barely known. Our data indicate only modest variation in Sr–Nd (Fig. 7a), Nd–Hf (Fig. 7b) or Pb isotopes (Figs. 7c–e) between mafic samples from the different regions of Armenia with the
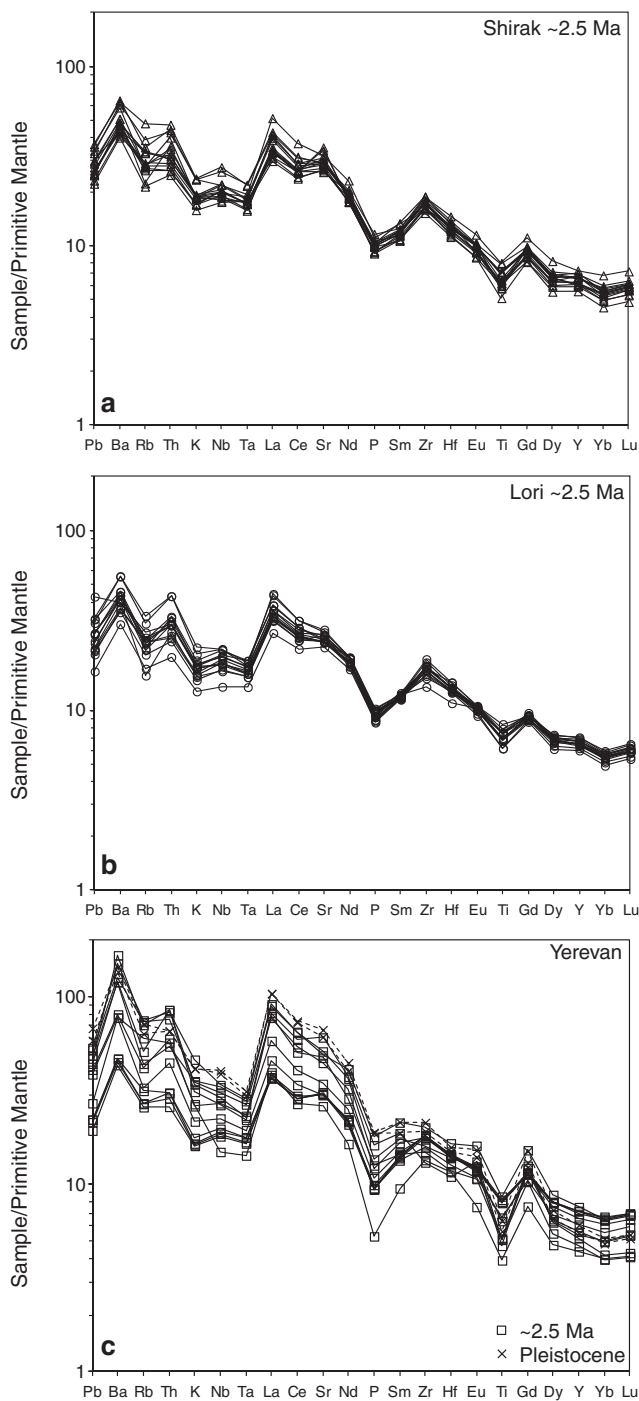
Fig. 6. a–c) Primitive Mantle-normalised trace element patterns (normalising values from Sun and McDonough, 1989).

exception of three samples. Firstly, one dolerite from Shirak (S14.4) has high $^{87}Sr/^{86}Sr$ (0.704775) (Fig. 7a). This sample was not analysed for Pb–Hf isotopes. Secondly, the least-evolved lava from Yerevan, Y8.1, also has high $^{87}Sr/^{86}Sr$ (0.704768) but also a high Th/Yb ratio (>3) coupled with the lowest $^{143}Nd/^{144}Nd$ of all the recent samples (Figs. 7a, 8a) and the second-highest $^{206}Pb/^{204}Pb$ ratio (Figs. 7b–e). Finally, a single sample from Lori (L8.3) has higher $^{143}Nd/^{144}Nd$ (0.512905) and considerably lower $^{206}Pb/^{204}Pb$ (18.705) compared with the other samples, but does not have unusually high Th/Yb (Fig. 8b).

We conclude that the trace element and isotope variations displayed by these three samples are the product of small amounts of crustal contamination by different crustal lithologies. Sample S14.4, with high

$^{87}Sr/^{86}Sr$ and low Th/Yb, was probably contaminated by Jurassic–Paleogene arc rocks with mostly low Th/Yb ratios (Figs. 8a, c). The Yerevan sample Y8.1, which has high $^{87}Sr/^{86}Sr$, Th/Yb and $^{206}Pb/^{204}Pb$ is more likely to have been contaminated by rocks within the South Armenian Block, which, given the Palaeozoic–Proterozoic age of this basement (Rolland et al., 2009 and references therein), are likely to be highly radiogenic. Finally, L8.3 from Lori Province has very low $^{206}Pb/^{204}Pb$, meaning that it plots close to the Jurassic and Upper Jurassic–Lower Cretaceous arc rocks on various figures and was probably contaminated by such basement lithologies (Figs. 7c, d; 8b–d). With the exception of these three samples, it seems that crustal contamination is not a significant process in the evolution of mafic Armenian collision magmas.

6.1.2. Contamination in more evolved samples from Shirak Province

Neill et al. (2013) concluded that there was insufficient evidence from Nd and Sr isotopes to judge if intermediate–felsic lavas and scoria cones from Shirak Province were contaminated by the local Mesozoic–Early Cenozoic arc basement or had simply evolved by fractional crystallisation and magma mixing. As the Jurassic–Paleogene arc rocks have distinct Pb isotope signatures compared to the recent mafic magmas (see Section 6.2.2. below for discussion of this feature) contamination effects may now be discussed. Considering data from the felsic Shirak rocks (see Supplementary Item C for data), there is a modest correlation between Pb isotopes and both Th/Yb (Fig. 7b) and SiO$_2$ (Fig. 8c), such that the least evolved samples have the highest Pb isotope ratios and these ratios become more akin to the Jurassic–Paleogene samples as the magmas evolve. Therefore, assimilation–fractional crystallisation (AFC) processes were likely to have been operating to a limited extent during the later stages of magmatic evolution.

6.2. Nature of the mantle source beneath Armenia

6.2.1. Major and trace element evidence for mantle source characteristics

All of the magmas have quite flat chondrite-normalised HREE patterns (Fig. 5). Of the common mantle minerals, garnet has $D_{Dy} < D_{Lu}$, so the presence of flat HREE patterns indicates that it is unlikely to have played a significant role as a residual phase during partial melting. The lack of garnet in the mantle source indicates partial melting of the shallow upper mantle at less than ~75 km (Robinson and Wood, 1998). Geochemical results are consistent with geophysical studies which show slow P- and S-wave velocities in the upper mantle at ~50 km depth (Piromallo and Morelli, 2003; Maggi and Priestley, 2005; Zor, 2008; Koulakov et al., 2012). When compared with typical mid-ocean ridge basalts, the samples have much higher HFSE/HREE and LREE/HREE ratios (e.g. Fig. 8a). This finding indicates that either the mantle source of the Armenian basalts was significantly more enriched in incompatible elements than DMM, and/or that the degree of partial melting beneath the 45 km-thick Armenian crust (Zor, 2008; Koulakov et al., 2012) was considerably lower than the ~5–15% expected for typical MORB-source mantle (Niu and Hékinian, 1997). Both conclusions are likely to be valid as lower-degree melting will preferentially sample more fertile and thus more incompatible element-enriched sources.

On a Th/Yb vs. Ta/Yb plot the incompatible element-enriched signature of the Shirak samples relative to MORB is obvious (Fig. 8a). Samples also have high Th/Yb ratios which are taken to reflect, in the absence of evidence for widespread crustal contamination, the presence of a subduction-modified mantle source. Further evidence for a subduction-modified source comes from the negative Nb–Ta anomalies on the normalised plots (Figs. 6a–c), reflecting retention of these HFSE in insoluble components such as rutile in the subducting slab (e.g. McCulloch and Gamble, 1991; Foley et al., 2000). It seems unlikely that an 'arc signature' would be derived from the convecting asthenosphere >10 Myr after slab break-off and up to ~30–35 Myr after the end of oceanic subduction. Therefore any subduction-like geochemical signature in the Pleistocene basalts is highly likely to have originated
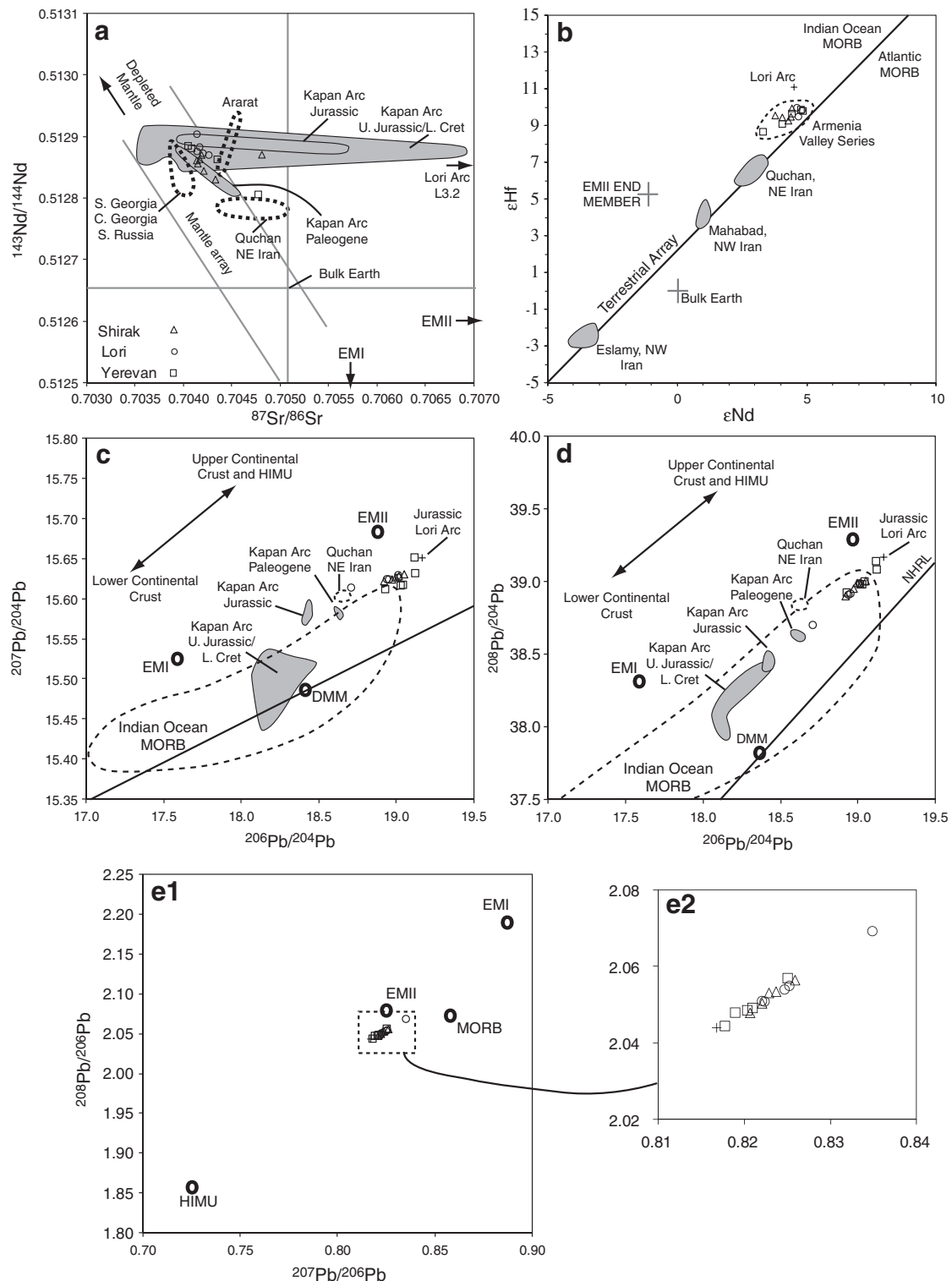
Fig. 7. Radiogenic isotope plots for mafic samples. Pre-Pliocene samples are not age-corrected as they are being used to investigate contamination effects in recent samples. a) $^{143}Nd/^{144}Nd$ vs. $^{87}Sr/^{86}Sr$. Mesozoic to Early Cenozoic arc rocks from the Kapan Zone, SE Armenia in this and all subsequent diagrams are from Mederer et al. (2013). Mantle Array and Bulk Earth as used in Rollinson (1993). b) εNd vs. εHf. EMII from Nowell et al. (1998). Terrestrial Array and Bulk Earth from Chauvel et al. (2008). Eslamy samples — Pang et al. (2013), Quchan — Kheirkhah et al. (in press), and Mahabad — Neill et al. (2013). Chondritic ratios used were: Nd − 0.512638 and Hf − 0.272772. c–d) $^{207}Pb/^{204}Pb$ vs. $^{206}Pb/^{204}Pb$ and $^{208}Pb/^{204}Pb$ vs. $^{206}Pb/^{204}Pb$. Indian Ocean MORB and the Northern Hemisphere Reference Line (NHRL) are from Ingle et al. (2002). e) $^{208}Pb/^{206}Pb$ vs. $^{207}Pb/^{206}Pb$ showing the position of the HIMU end member. Mantle end members on c) to e) are from Saal et al. (2005).

by melting within the subduction-modified lithospheric mantle. Neill et al. (2013) pointed out that even the least-evolved samples had arc-like negative Nb–Ta anomalies on normalised plots, which did not diminish with increasing Mg#. Therefore, no high-Nb–Ta asthenospheric components could be identified.

6.2.2. Isotopic constraints on the Armenian mantle source

Recent Armenian collision magmas have more radiogenic Pb isotope characteristics compared to the Jurassic–Paleogene Arc of the Lesser Caucasus (Figs. 7c–d). Assuming the lithospheric mantle beneath Armenia stabilised during or immediately after magmatism in the Arc
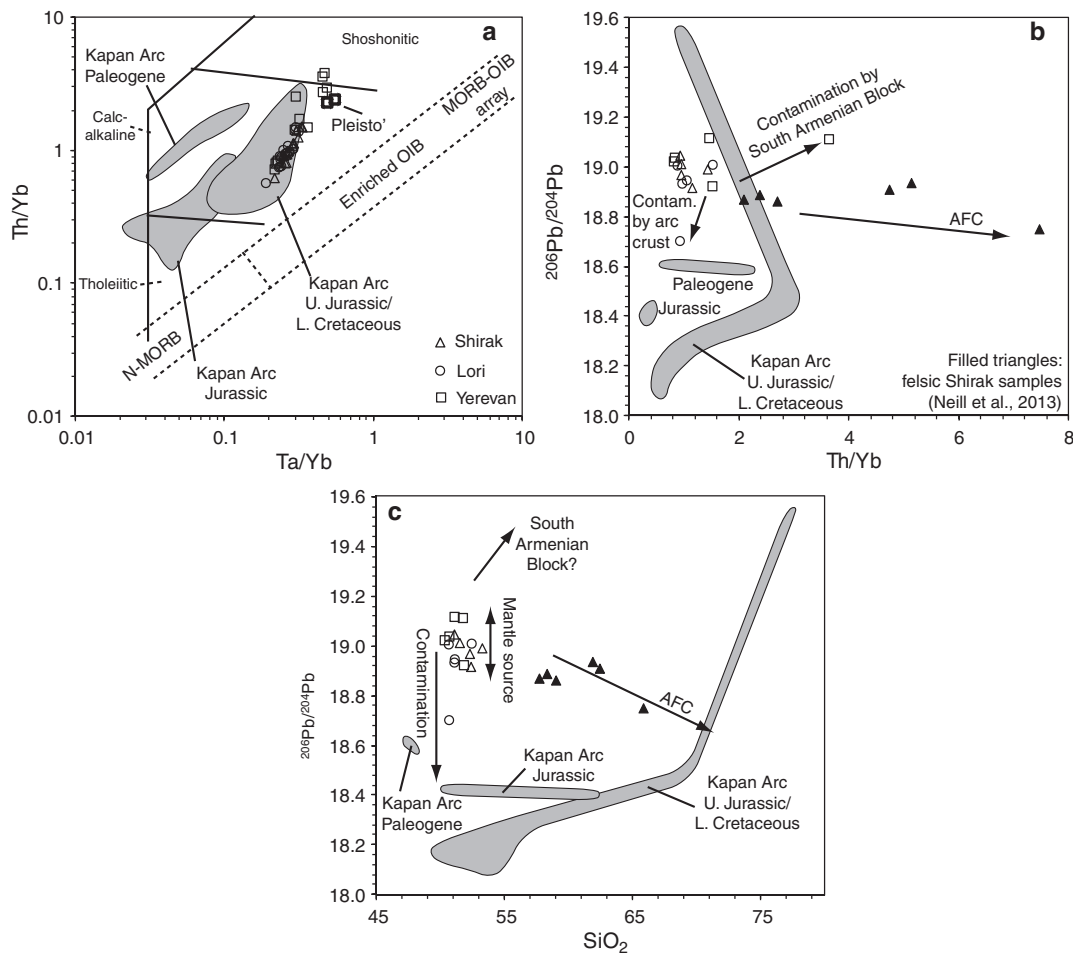
Fig. 8. Trace element and isotopic evidence for crustal interaction. Jurassic–Paleogene Kapan Arc data from Mederer et al. (2013). (a) Th/Yb vs. Ta/Yb diagram from Pearce (1983). (b) $^{206}Pb/^{204}Pb$ vs. Th/Yb and (c) $^{206}Pb/^{204}Pb$ vs. SiO$_2$, showing the effect of crustal contamination and fractional crystallisation on the isotopic composition of magmas erupted through the Arc of the Caucasus and the South Armenian Block. Filled triangles in (b) and (c) are felsic rocks from Shirak Province which are genetically related to the mafic Shirak lavas and show more evidence for crustal contamination compared to the mafic samples. Data from Neill et al. (2013) and this work (Supplementary Item B).

of the Lesser Caucasus, the mantle should have initially had the same isotopic composition as the complementary arc rocks. Since the Mesozoic and Early Cenozoic, the lithospheric mantle will then have evolved isotopically prior to the melting events which formed the <3 Ma collision magmas. The extent of radiogenic in-growth strongly depends on the U, Pb and Th concentrations of the mantle source. Any mantle metasomatism would affect the rate of in-growth or cause variations in different Pb isotope systems. Nevertheless, Rooney et al. (2014) calculated that $^{206}Pb/^{204}Pb$ ratios in ambient depleted mantle evolve by ~1 point in 500 Myr, too slow to account for the variation between the Armenian dolerites and the older arc rocks. Subduction-modified lithosphere was argued to evolve slightly quicker, with a change of 1 point in $^{206}Pb/^{204}Pb$ ratios taking ~300 Myr, again too slow for Armenia.

There are no Armenian mantle xenoliths and thus no U, Pb and Th concentrations to assign to a mantle source. We modelled mantle isotopic evolution using initial Pb isotope ratios of the aforementioned Kapan Zone rocks as representative of 'typical' mantle sources at their time of eruption (Mederer et al., 2013). These sources were aged to recent times using concentrations of U, Pb and Th in metasomatised mantle xenoliths from Spitsbergen (Ionov et al., 2002; see Section 6.3 below for discussion on these samples). Results from this aging process are shown in Fig. 9, demonstrating that aged sources have similar or much higher Pb isotope ratios compared to the Pleistocene samples. The limited number of older arc samples, lack of constraint on mantle composition and the possibility of

crustal contamination in both the arc and the collision magmas preclude detailed assessment of the age of the sub-Armenian mantle. Nevertheless the Armenian dolerites could feasibly be derived from a mantle source of Jurassic, Cretaceous or Palaeogene age, notwithstanding any metasomatic effects.

It is also possible that the sub-Armenian lithosphere has been metasomatised by small-degree asthenospheric melts since the Palaeogene. Small volume melts may not wipe out the arc-like trace element signature of the Armenian mantle but may alter its isotopic composition. The Armenian samples are quite clustered in isotope space (Figs. 7, 8). Hence there is no undeniable isotopic evidence for interaction between Armenian lithospheric mantle and asthenospheric melts. However, there are no constraints on the isotopic composition of the Anatolian–Caucasian asthenosphere. Another possible explanation for the observed isotopic variation between the older arc rocks and the recent collision magmas is that during the final stages of Neo-Tethyan subduction the Bitlis slab continued dewatering until the slab break-off event. Subduction may also have included the thinned continental passive margin of Arabia (e.g., Allen et al., 2013). Fluids derived from Arabian Platform sediments, ultimately reflecting juvenile Pan-African continental crust, may have high Pb isotope ratios, leading to a fertilised sub-Armenian mantle significantly more radiogenic than that responsible for the preceding arc magmatism. Like Ekici et al. (2014), we recognise that there are few if any appropriate elemental and isotopic studies of the Arabian Platform with which to test this hypothesis.
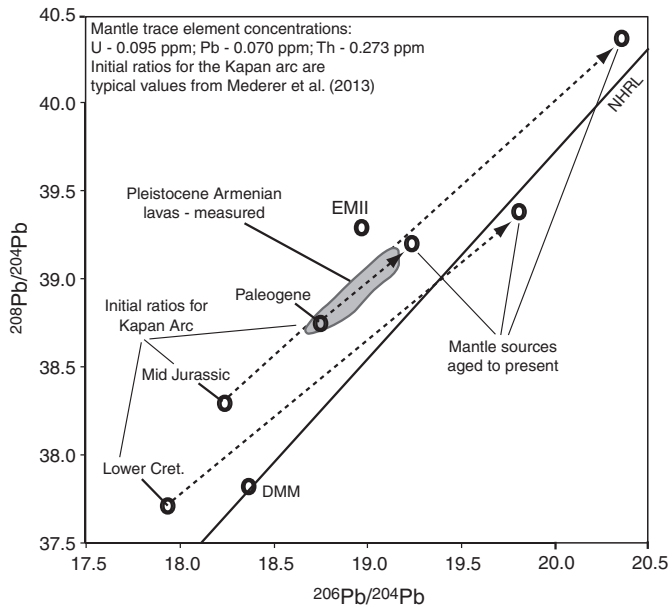
Fig. 9. Initial Pb isotope ratios of Jurassic, Cretaceous and Palaeogene arc-related samples from southern Armenia (Mederer et al., 2013) are used to reflect the composition of the Armenian lithospheric mantle at the time of arc magmatism. These samples are aged using appropriate U–Pb–Th concentrations (Ionov et al., 2002) in order to judge the present-day composition of sub-Armenian mantle of Jurassic, Cretaceous and Palaeogene age. Sources for calculations: Pb atomic weights — de Laeter et al. (2003); U and Th atomic weights — Wieser (2006); relative isotopic abundances of U and Th — Rosman and Taylor (1998); and decay constants — Steiger and Jager (1977).

6.3. Partial melting model for the Pleistocene lavas

Depletion of the Armenian mantle source during the Mesozoic to Early Cenozoic by melting, and subsequent re-fertilisation by any subduction-related fluids or asthenospheric melts will have altered the mineralogy of the source relative to lherzolitic mantle. Depleted MORB-source mantle (e.g. Workman and Hart, 2005) is therefore not an appropriate starting composition for melting models. Some authors (e.g. Özdemir and Güleç, 2014) based models on an enriched 'primitive' mantle source.

We have used well-characterised depleted spinel harzburgite xenoliths from Spitsbergen (Ionov et al., 2002) to construct a partial melting model (Fig. 10). Several Spitsbergen xenoliths are metasomatised: they contain a few wt.% amphibole, and have subduction-like La/Nb ratios (>1). A non-modal batch melting model (Shaw, 2005) was constructed using the mineral proportions of a relevant Spitsbergen harzburgite xenolith, the partition coefficients of Ionov et al. (2002) and our own melt modes. The choice of initial concentrations of trace elements (C_0) was based at first on the peridotite samples and computed values of Ionov et al. (2002) and then changed iteratively within the range presented by depleted MORB mantle (Workman and Hart, 2005) and enriched oceanic plateau-like (Fitton and Godard, 2004) mantle sources. These changes were designed to reflect potential source heterogeneity for the Armenian magmas, and the effect of addition of small volumes of melt and/or fluid from the asthenosphere or a Tethyan slab. We modelled selected REE and HFSE concentrations and present our results for 1–5% partial melting in Fig. 10 along with best-fit models for the least-evolved Shirak/Lori and Yerevan samples in Table 3. Lavas from Shirak and Lori have similar trace element geochemistry (Section 4.2)
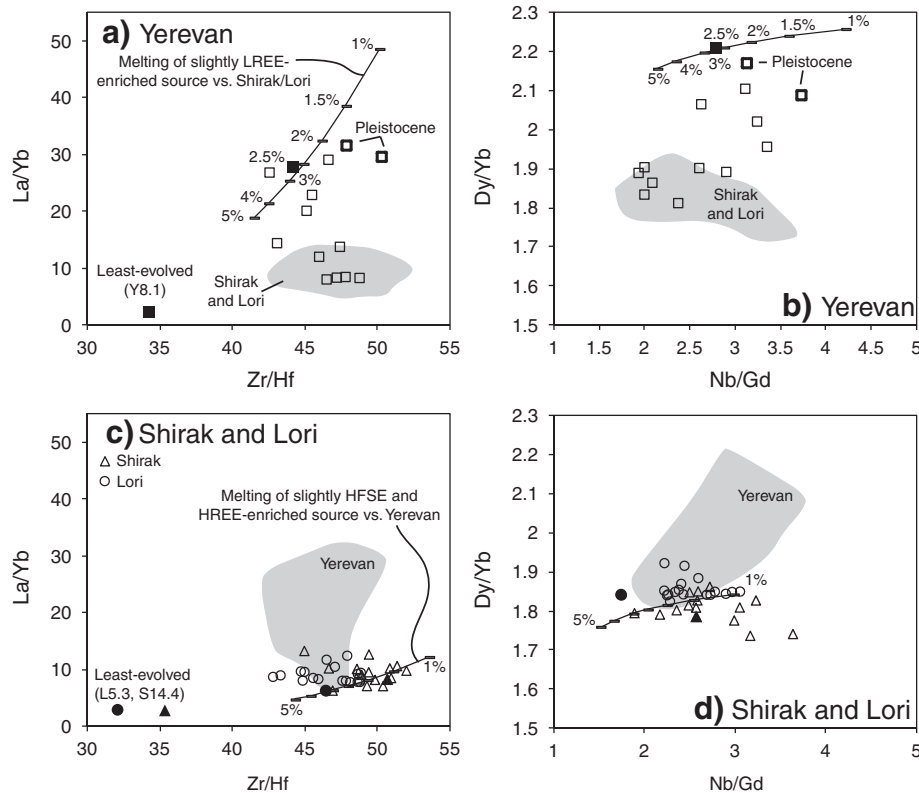

Fig. 10. Partial melting curves with differing starting compositions within the range of DMM and oceanic plateau sources, demonstrating that the least-evolved samples from each location can be explained by ~1.5–3% non-modal partial melting of heterogeneous metasomatised, amphibole-bearing peridotite. See Section 6.4 and Table 3 for more details and discussion. Ticks on melting curves (c) and (d) are at the same intervals as on (a) and (b).

Table 3
Non-modal batch melting model incorporating 20% fractional crystallisation of olivine + spinel in the ratio 90:10 (after Shaw, 2005). Source mode is from Spitsbergen peridotite sample 318 (Ionov et al., 2002). Starting compositions were modified after values in Ionov et al. (2002) and are tailored for the Yerevan and Shirak/Lori suites. The Yerevan source is modelled to be more enriched in LREE compared to Shirak/Lori, the Shirak/Lori source slightly enriched in HREE and HFSE compared to Yerevan. The changes made are all within the range of natural peridotites and calculated mantle sources (DMM and oceanic plateau source). The differences between sources imply a slightly smaller degree of melting for Yerevan, and a slightly more fertile source for Shirak/Lori.

	Olivine		Orthopyroxene		Clinopyroxene		Amphibole		Spinel	Sum
Source mode	0.794		0.123		0.03		0.042		0.011	1
Melt mode	0.15		0.15		0.22		0.42		0.06	1
		La	Gd	Dy		Yb	Zr		Hf	Nb
Starting composition (ppm)										
For Yerevan		1.2	0.3	0.2		0.1	4		0.105	0.48
For Shirak and Lori		0.5869	0.321	0.317		0.202	7		0.172	0.3635
Kd values										
Olivine		0.0001	0.00076	0.0014		0.00364	0.004		0.006	0.0002
Orthopyroxene		0.0002	0.0128	0.0261		0.0986	0.005		0.01	0.0005
Clinopyroxene		0.054	0.4	0.442		0.427	0.13		0.2	0.0077
Amphibole		0.086	0.64	0.707		0.683	0.156		0.24	0.2
Spinel		0.0004	0.00042	0.0004		0.00053	0.005		0.01	0.001
Non-modal batch melting (ppm)										
For Yerevan at 2.5% melting										
Initial result		41.2	5.3	3.2		1.4	108.4		2.4	15.1
After Rayleigh fractionation		51.5	6.6	4.0		1.8	135.4		3.0	18.9
				Final La/Nb = 2.7			Final Zr/Hf = 44.9			
For Shirak and Lori at 3% melting										
Initial result		17.3	5.3	4.9		2.7	169.0		3.6	10.0
After Rayleigh fractionation		21.6	6.7	6.1		3.4	211.0		4.5	12.5
				Final La/Nb = 1.7			Final Zr/Hf = 46.9			
Comparison with samples (ppm)										
Y8.1, least-evolved, Yerevan		53.0	6.8	4.2		1.9	137.0		3.1	19.0
L5.3, least-evolved, Lori		18.5	5.5	5.4		2.9	192.1		4.1	9.7

so they are treated as one series. Each partial melting curve has been corrected for 20% Rayleigh fractional crystallisation (Shaw, 2005) of an assemblage of olivine and spinel in the ratio 9:1.

Low-degree partial melting (<5%) of a hydrous, metasomatised source can generate similar elemental concentrations and ratios to the least-evolved samples from Yerevan and Shirak/Lori, assuming that REE and HFSE concentrations in the real samples have not been severely altered by contamination. We used 2.5% partial melting for Yerevan and 3% for Shirak and Lori, with C_0 for each trace element being altered slightly for the different localities: higher initial LREE concentrations were used for the Yerevan samples, and higher initial HREE and HFSE concentrations were used for Shirak/Lori, relative to the other region(s) (Table 3). It could be argued that the Yerevan samples formed by lower degree melting of a more metasomatised, but depleted mantle source; whilst the Shirak/Lori samples had a less depleted mantle source and higher degrees of partial melting relative to Yerevan. The Upper Pleistocene samples appear to be those derived from the smallest amounts of partial melting. This finding may indicate that recent melting beneath this small part of Armenia peaked during the Lower Pleistocene before tailing off during the Upper Pleistocene.

6.4. Geodynamics of the Turkish–Iranian Plateau

6.4.1. Tethyan slab break-off

We now attempt to link our findings to geodynamic models for the region. The timing of break-off processes beneath Eastern Anatolia and the Caucasus in the Late Cenozoic is not well understood (e.g., Skolbeltsyn et al., 2014). Most papers infer Eocene break-off of a north-dipping slab beneath the Pontides (e.g., Keskin et al., 2008; Sosson et al., 2010) which implies that the Pontide slab had no role in Pliocene–Quaternary magmatism. In contrast, a much later Miocene break-off of a north-dipping Pontide slab beneath the Lesser Caucasus (close to the Sevan–Akera Suture Zone), as suggested by recent seismic data (Skolbeltsyn et al., 2014), would be penecontemporaneous with break-off beneath the more southerly Bitlis Suture and should result in a very wide zone of asthenospheric upwelling which might better

explain the Late Miocene onset of collision magmatism in Eastern Anatolia, Armenia and Georgia.

Nevertheless, the Armenian samples have been erupted at least 10–15 Myr after the argued time of Neo-Tethyan break-off (Keskin, 2003; Pang et al., 2013; Skolbeltsyn et al., 2014). This makes it difficult to attribute recent Armenian magmatism directly to break-off, especially as magmatism appears to have intensified in the last 3 Myr without contemporaneous evidence for a trigger such as crustal extension. In break-off scenarios, models show convecting mantle welling up into a narrow zone beneath collision zones (Davies and von Blanckenburg, 1995), but there are no constraints on how persistent the upwelling is or what volume of asthenosphere may be 'stirred up' by break-off processes, particularly if the slab had a flat geometry prior to break-off (e.g., Skolbeltsyn et al., 2014). It remains unproven if Pleistocene magmatism in Armenia is directly related to Neo-Tethys break-off.

The break-off event may nevertheless be significant from a geochemical point of view. Between the initial collision and break-off (Oligocene to Early Miocene), much of the Turkish–Iranian Plateau experienced only low levels of magmatic activity (Chiu et al., 2013) indicating that mantle melting was not widespread despite the presence of one (Bitlis) or two (Bitlis and Pontide) slabs beneath the region. These slabs could heat up and dewater, lowering the viscosity of the mantle beneath Armenia. Upon break-off, the hydrated, weak lithosphere beneath the plateau may be capable of undergoing delamination, as discussed in the next section.

6.4.2. Can small-scale delamination events explain recent Armenian magmatism?

It has already been highlighted that magmatism has persisted and even increased in volume long after break-off. Kaislaniemi et al. (2014) proposed that such longevity could be explained by localised excision of mantle lithosphere driven by small-scale convection cells in the upper asthenosphere. This proposal was based on numerical simulations with an initial setup consisting of 100 km thick lithosphere and mantle hydration of the order of a few hundred ppm of H_2O, stored in nominally anhydrous minerals such as olivine, as a relic from the

prior subduction history of the region. Mantle hydration results in a lowering of its viscosity (e.g., Hirth and Kohlstedt, 2003) therefore promoting small-scale convection in the absence of crustal extension. Kaislaniemi et al.'s model predicted delamination of <100 km wide blocks of lithosphere, at random locations, with delamination repeat times of a few to several tens of Myr depending on the extent of mantle hydration. A few per cent melting of asthenosphere was predicted due to upwelling of the asthenosphere into pockets vacated by delaminated lithosphere.

Geochemical evidence presented here (Section 6.2.1) points towards recent melting of lithospheric and not asthenospheric mantle beneath Armenia. Given that the Armenian crust is ~45 km thick (Zor, 2008; Koulakov et al., 2012) and is underlain by at least a thin lithospheric mantle lid, significant amounts of asthenospheric melting may have been suppressed. It is also likely that the most fusible phases lie in the lithospheric mantle in the form of hydrous, subduction-modified amphibole-bearing pyroxenites and pyroxene-rich peridotites. Many experimental studies have been conducted on nominally anhydrous peridotites and pyroxenites (e.g., Baker et al., 1995; Walter, 1998; Presnall et al., 2002; Pertermann and Hirschmann, 2003; Lambart et al., 2009). These experiments have demonstrated that typical pyroxenites at pressures from 1–3 GPa have solidi ~50–200°C lower than peridotites. It is expected that the solidus temperature of subduction-modified, hydrated, metasomatised material in the lithospheric mantle will be considerably lower than for nominally anhydrous asthenosphere.

Therefore, a form of sublithospheric small-scale convection, modified to account for preferential melting of hydrous pyroxenitic lithologies in the lithosphere (e.g., Hirth and Kohlstedt, 1996), can potentially explain the most recent collision magmatism seen across the Turkish–Iranian Plateau. Our model for recent melting beneath the collision zone is therefore presented in Fig. 11. The cross-section shows tens of km-scale lithospheric drips beneath the collision zone in Armenia and subsequent asthenospheric upwelling. This is argued to result in lower lithosphere heating, dewatering of the detached lithosphere and initiation of partial melting in newly-metasomatised upwelling asthenosphere as well as the lower lithosphere. The figure

also highlights melting mechanisms proposed for other parts of the Turkish–Iranian Plateau, as discussed by Neill et al. (2013), with the addition of thick lithosphere beneath the Kura Basin based on geophysical results (Skolbeltsyn et al., 2014).

6.5. A brief note on collision magmatism and the continental crust

Collisional volcanic and plutonic rocks are common spatially and temporally on Earth. Typical examples include the Late Cenozoic Tibetan Plateau (Niu et al., 2013); the Permian to Early Jurassic Altaids of China (Wu et al., 2002); the Palaeozoic Scottish Caledonides (Fowler et al., 2008) and arguably Archaean sanukitoid terranes (Fowler and Rollinson, 2012), indicating that collision magmas have high preservation potential so they should have a long-term effect on crustal composition (e.g., Niu et al., 2013). Many authors consider continental crust to be born in supra-subduction environments, given that oceanic arcs have similar LILE-LREE/HFSE characteristics compared to continental crust (Kelemen et al., 2003; Rudnick and Gao, 2003). Arc terranes must be later modified by continental margin magmatism, collision, delamination and infra-crustal recycling to drive bulk compositions towards the andesitic, high Th/La flavour of continental crust (e.g. Plank, 2005; Davidson and Arculus, 2006). Niu et al. (2013) argued that felsic collision magmatism is geochemically similar to bulk continental crust, but there is no contemporary argument about mafic collision zone magmas and their trace element budget. Recent mafic lavas of Armenia and the wider Turkish–Iranian Plateau, often with little evidence for crustal contamination, are good examples to discuss what effect the mantle-derived component of collision magmatism has on the continents. It is also pertinent to ask if the Turkish-Iranian Plateau is a 'typical' orogenic belt. Şengör and Okuroğullari (1991) and Şengör and Natal'in (1996) used the term "Turkic-type orogen" to describe mountain belts with moderate crustal thicknesses and thin lithosphere which had experienced slab break-off. They argued that such orogenic belts have long existed and may have dominated the Archaean record. Indeed, processes such as slab break-off were likely to have been more common and to have occurred at shallower depths in the Archaean
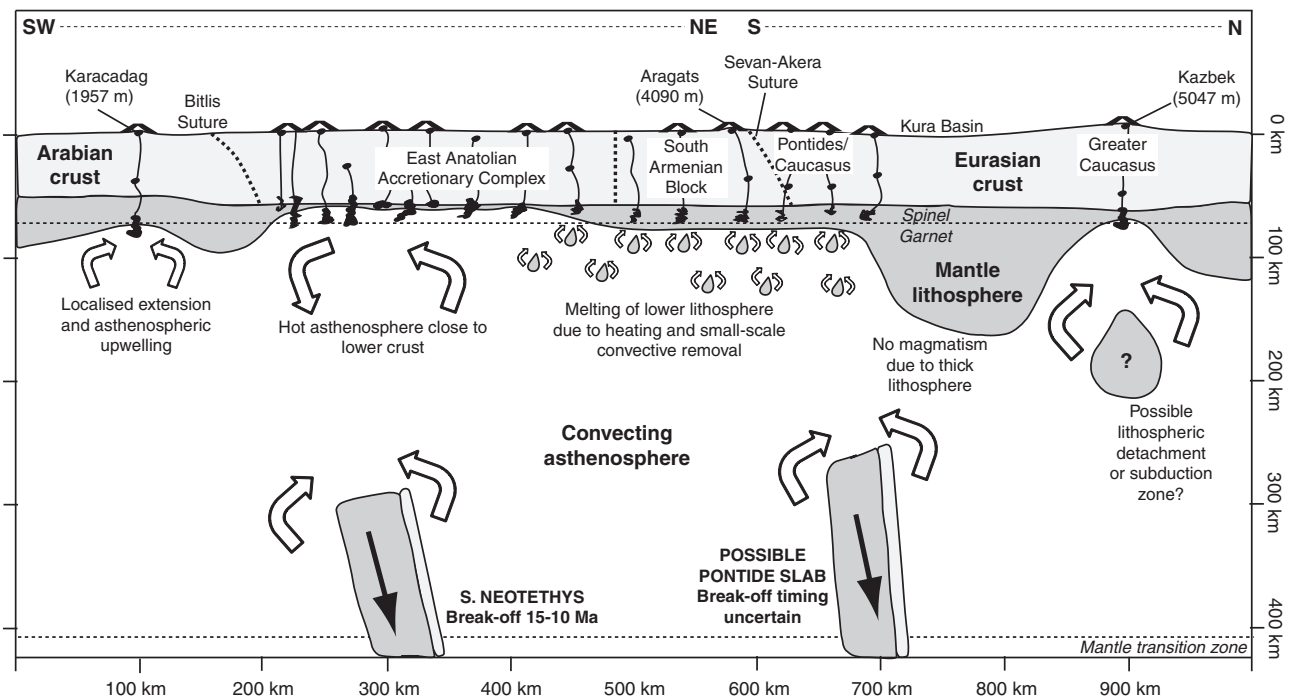

Fig. 11. Geodynamic model showing the lithosphere and upper mantle beneath the Arabia–Eurasia collision zone through Eastern Turkey, Armenia, Georgia and southern Russia, modified after Neill et al. (2013) and Kaislaniemi et al. (2014). The cross-section changes in orientation in Armenia and the approximate line of section is on Fig. 2a. Crustal thicknesses and implications of subducted slabs are adapted from Zor (2008) and Skolbeltsyn et al. (2014) and lithospheric thicknesses from numerous works including Angus et al. (2006). Note that Mumladze et al. (2015) have recently proposed magmatism in the Greater Caucasus to relate to a further north-dipping subduction zone beneath this region.

Table 4
Average incompatible trace element composition of mafic magmas (<55 wt.% SiO_2) from across Armenia (Neill et al., 2013, this study) and the whole Turkish–Iranian Plateau (GEOROC database; http://georoc.mpch-mainz.gwdg.de/georoc; Allen et al., 2013; Kheirkhah et al., 2013, in press; Özdemir and Güleç, 2014). Results are compared with average continental crust (Rudnick and Gao, 2003) and the average composition of calc-alkaline arcs (Kelemen et al., 2003). See Section 6.5. for discussion.

	Armenia (ppm) $\pm 1\sigma$	n	Felsic, Shirak–Armenia $\pm 1\sigma$	n	TIP (ppm) $\pm 1\sigma$	n	Continental crust	Calc-alkaline arcs (Alaska)
Th	3.3 ± 1.3	46	6.7 ± 1.7	21	8.5 ± 6	484	5.8	2.0
La	30 ± 13	46	30 ± 3.5	21	40 ± 29	461	20	12
Nb	15 ± 4	46	13 ± 2	21	23 ± 16	515	8	6
Ta	0.8 ± 0.1	46	0.7 ± 0.1	21	1.6 ± 1.3	248	0.7	0.5
Zr	188 ± 19	46	176 ± 19	21	224 ± 92	515	132	93
Hf	4.0 ± 0.3	46	3.9 ± 0.4	21	5.2 ± 2.3	277	3.7	2.1
Th/La	0.1		0.2		0.2		0.3	0.2
La/Nb	2.0		2.3		1.7		2.5	2.0
Zr/Hf	47		45		43		36	44
Nb/Ta	20		18		14		11	12

and Proterozoic than at present (e.g., van Hunen and Allen, 2011; Sizova et al., 2014). If this is the case, Turkish–Iranian collision magmatism should be a good analogue for tracking the effect of such magmatic activity on long-term crustal evolution.

Space does not permit a detailed discussion, but we note that analyses of mafic collision magmas (<55 wt.% SiO_2) from Armenia and the Turkish–Iranian Plateau have ~1.5–3 times the incompatible element budget of bulk continental crust (Table 4). Low-volume collision magmatism may therefore add a 'flavour' to the continental crust without significantly affecting its major element composition. Magmatism related to the Arabia–Eurasia collision also has similar or higher Zr/Hf, Nb/Ta and La/Nb compared to bulk continental crust (Table 4; Fig. 12). However, bulk continental crust and upper crust has very high Th/La (~0.25–>0.3) relative to mafic Turkish–Iranian Plateau magmatism (Th/La ~ 0.2) but especially Armenia (Th/La ~ 0.1) (Table 4; Fig. 12).
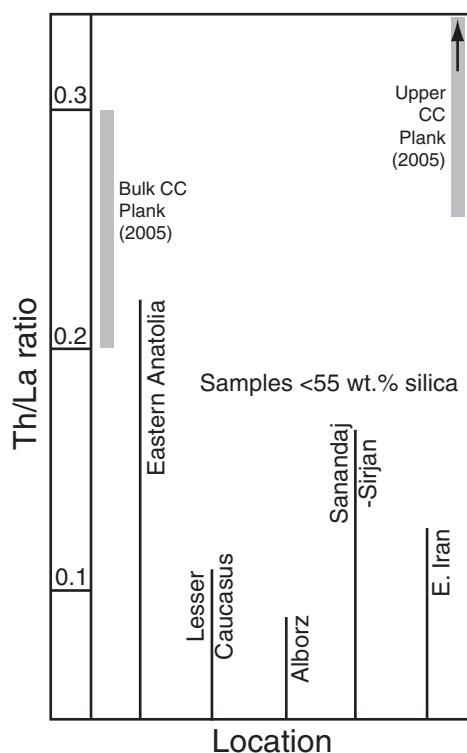

Fig. 12. Approximate Th/La ratios of mafic (<55 wt.%) volcanic rocks of the Turkish–Iranian Plateau, grouped geographically. Results show that collision magmas which erupted through the East Anatolian Accretionary Complex have the highest, most continental crust-like Th/La ratios, probably as a result of extensive contamination during magma ascent. In spite of this, the mafic mantle-derived component of collision magmatism appears to have a low Th/La signature. Less-contaminated samples from the Lesser Caucasus, Alborz Mountains and Eastern Iran have very low Th/La ratios unlike continental crust. Data sources: Table 4.

High Th/La ratios in the continental crust may be driven by the removal of low Th/La mafic material (cumulates and granulites) from the lower crust by foundering during continental margin magmatism or collision (Plank, 2005). The felsic Ridge Series samples from Shirak in Armenia have Th/La ranging from 0.16 to 0.32 (Neill et al., 2013; Table 4), so even if such felsic rocks were to dominate the magmatic record, it seems that their differentiation history cannot help generate very high Th/La ratios. We speculate that foundering is required, not only to balance the addition of low Th/La components from accreted arcs, but also to account for the addition of low Th/La mantle-derived collision magmas.

7. Conclusions

- Magmatism is a persistent widespread feature of the Turkish–Iranian Plateau, 25–30 Myr after initial collision and 10–15 Myr after break-off of the southern Neo-Tethys slab. The precise cause of this magmatism is debated. Southern Neo-Tethys break-off is not an entirely satisfactory trigger for partial melting of the mantle in regions far from the suture such as Armenia, or for the most recent magmatic activity more generally.

- Some Pleistocene mafic alkaline lavas from across Armenia have elemental and isotopic evidence for contamination by Mesozoic–Paleogene arc or older South Armenian Block crust. However, the vast majority of mafic magmas have experienced little or no assimilation so they can be used to indicate the composition and melting characteristics of the sub-Armenian lithosphere following the termination of Tethyan subduction.

- Geochemical results are compatible with low-degree partial melting of a subduction-modified lithospheric mantle source within the spinel stability field.

- Stirring of the convective mantle due to slab break-off of either the southern Neo-Tethys (Bitlis) slab or the northern (Pontide) slab may have aided asthenospheric upwelling and the onset of collision magmatism beneath Armenia in the Late Miocene. Whole-scale lithospheric delamination is an unlikely aid, however, as there are no large-scale spatial or temporal patterns in volcanism related to diachronous removal of lithosphere, nor evidence for extensive lower crustal melting. We argue that small-scale convective removal of the lowermost lithosphere and replacement by convecting asthenosphere (e.g., Kaislaniemi et al., 2014) is an effective mechanism for heating and partial melting of fusible, subduction-modified components within the lithospheric mantle, which can persist for many millions of years after slab break-off.

- Collision magmatism contributes to bulk continental crust. However, mafic collision magmas in Armenia have LREE and HFSE concentrations double that documented in continental crust, as well as distinctive low Th/La signatures. Even if collision zone magmatism is volumetrically minor in comparison to subduction- and rift-related magmatism, its distinctive incompatible element

'flavour' needs to be accounted for in models of crustal composition and evolution.

Appendix A. Supplementary data

Supplementary data to this article can be found online at http://dx.doi.org/10.1016/j.chemgeo.2015.03.013.

References

Adamia, S.A., Chkhotua, T., Kekelia, M., Lordkipanidze, M., Shavishvili, I., 1981. Tectonics of the Caucasus and adjoining regions: implications for the evolution of the Tethys ocean. J. Struct. Geol. 3, 437–447.

Adamia, S.A., Zakariadze, G., Chkhotua, T., Sadradze, N., Tsereteli, N., Chabukiani, A., Gventsadze, S., 2011. Geology of the Caucasus: a review. Turk. J. Earth Sci. 20, 489–544.

Allen, M.B., Armstrong, H.A., 2008. Arabia–Eurasia collision and the forcing of mid-Cenozoic global cooling. Palaeontol. Palaeoclimatol. Palaeoecol. 265, 52–58.

Allen, M.B., Kheirkhah, M., Emami, M.H., Jones, S.J., 2011. Right-lateral shear across Iran and kinematic change in the Arabia–Eurasia collision zone. Geophys. J. Int. 184, 555–574.

Allen, M.B., Kheirkhah, M., Neill, I., Emami, M.H., McLeod, C.L., 2013. Generation of arc and within-plate chemical signatures in collision zone magmatism: Quaternary lavas from Kurdistan Province, Iran. J. Petrol. 54, 887–911.

Angus, D.A., Wilson, D.C., Sandvol, E., Ni, J.F., 2006. Lithospheric structure of the Arabian and Eurasian collision zone in eastern Turkey from S-wave receiver functions. Geophysical Journal International 166, 1335–1346.

Arutyunyan, E.V., Lebedev, V.A., Chernyshev, I.V., Sagatelyan, A.K., 2007. Geochronology of Neogene–Quaternary volcanism of the Geghama Highland (Lesser Caucasus, Armenia). Dokl. Earth Sci. 416, 1042–1046.

Babeyko, A.Yu., Sobolev, S.V., Trumbull, R.B., Oncken, O., Lavier, L.L., 2002. Numerical models of crustal-scale convection and partial melting beneath the Altiplano–Puna plateau. Earth Planet. Sci. Lett. 199, 373–388.

Baker, M.B., Hirschmann, M.M., Ghiorso, M.S., Stolper, E.M., 1995. Compositions of near-solidus peridotite melts from experiments and thermodynamic calculations. Nature 375, 308–311.

Balog, S., Baghdasaryan, G., Karapetyan, K., Pechkam, Z., Arva-Shosh, E., Ghukasyan, R., 1990. K–Ar dating of Upper-Pliocene–Quaternary volcanic rocks of Armenia. Earth Sci. Lett. 43, 24–38 (in Russian).

Best, M.G., Barr, D.L., Christiansen, E.H., Gromme, S., Deino, A.L., Tingey, D.G., 2009. The Great Basin Altiplano during the middle Cenozoic ignimbrite flareup: insights from volcanic rocks. Int. Geol. Rev. 51, 589–633.

Bird, P., 1978. Initiation of intracontinental subduction in the Himalaya. J. Geophys. Res. 83 (B10), 4975–4987.

Bottrill, A.D., van Hunen, J., Allen, M.B., 2012. Insight into collision zone dynamics from topography: numerical modelling results and observations. Solid Earth 3, 387–399.

Chauvel, C., Lewin, E., Carpentier, M., Arndt, N.T., Marini, J.-C., 2008. Role of recycled oceanic basalt and sediment in generating the Hf–Nd mantle array. Nat. Geosci. 1, 64–67.

Chernyshev, I.V., Lebedev, V.A., Arakleyants, M.M., Jrbashyan, R.T., Ghukasyan, Y.G., 2002. Geochronology of the Aragats volcanic centre, Armenia: evidence from K/Ar dating. Dokl. Earth Sci. 384, 393–398 (in Russian).

Chiu, H.-Y., Chung, S.-L., Zarrinkoub, M.H., Mohammadi, S.S., Khatib, M.M., Iizuka, Y., 2013. Zircon U-Pb age constraints from Iran on the magmatic evolution related to Neotethyan subduction and Zagros orogeny. Lithos 162, 70–87.

Cohen, K.M., Finney, S.C., Gibbard, P.L., 2013. The ICS International Chronostratigraphic Chart. Episodes 36, 199–204.

Davidson, J.P., Arculus, R.J., 2006. The significance of Phanerozoic arc magmatism in generating continental crust. In: Brown, M., Rushmer, T. (Eds.), Evolution and Differentiation of the Continental Crust. Cambridge University Press, Cambridge, pp. 135–172.

Davies, J.H., von Blanckenburg, F., 1995. Slab breakoff: a model of lithosphere detachment and its test in the magmatism and deformation of collisional orogens. Earth Planet. Sci. Lett. 129, 85–102.

de Laeter, J.R., Bohlke, J.K., de Bievre, P., Hidaka, H., Peiser, H.S., Rosman, K.J.R., Taylor, P.D.P., 2003. Atomic weights of the elements: review 2000. Pure Appl. Chem. 75, 683–800.

Dilek, Y., Imamverdiyev, N., Altunkaynak, Ş., 2010. Geochemistry and tectonics of Cenozoic volcanism in the Lesser Caucasus (Azerbaijan) and the peri-Arabian region: collision induced mantle dynamics and its magmatic fingerprint. Int. Geol. Rev. 52, 536–578.

Dowall, D.P., Nowell, G.M., Pearson, D.G., 2007. Chemical pre-concentration procedures for high-precision analysis of Hf/Nd/Sr isotopes in geological materials by plasma ionisation multi-collector mass spectrometry (PIMMS) techniques. In: Holland, J.G., Tanner, S.D. (Eds.), Plasma Source Mass Spectrometry: Applications and Emerging Technologies. The Royal Society of Chemistry, Cambridge, pp. 321–337.

Ekici, T., Macpherson, C.G., Otlu, N., Fontignie, D., 2014. Foreland magmatism during the Arabia–Eurasia collision: Pliocene–Quaternary activity of the Karacadağ Volcanic Complex, SW Turkey. J. Petrol. 55, 1753–1777.

Elkins-Tanton, L.T., 2007. Continental magmatism, volatile recycling, and a heterogeneous mantle caused by lithospheric gravitational instabilities. J. Geophys. Res. 112. http://dx.doi.org/10.1029/2005JB004072 (B03405).

England, P.C., Thompson, A.B., 1984. Pressure–temperature–time paths of regional metamorphism, I. Heat transfer during the evolutions of regions of thickened continental crust. J. Petrol. 25, 894–928.

Fitton, J.G., Godard, M., 2004. Origin and evolution of magmas on the Ontong Java Plateau. In: Fitton, J.G., Mahoney, J.J., Wallace, P.J., Saunders, A.D. (Eds.), Origin and Evolution of the Ontong Java Plateau. vol. 229. Geological Society of London Special Publication, pp. 151–178.

Foley, S.F., Barth, M.G., Jenner, G.A., 2000. Rutile/melt partition coefficients for trace elements and an assessment of the influence of rutile on the trace element characteristics of subduction zone magmas. Geochim. Cosmochim. Acta 64, 933–938.

Fowler, M., Rollinson, H., 2012. Phanerozoic sanukitoids from Caledonian Scotland: implications for Archean subduction. Geology 40, 1079–1082.

Fowler, M.B., Kocks, H., Darbyshire, D.P.F., Greenwood, P.B., 2008. Petrogenesis of high Ba–Sr plutons from the Northern Highland Terrane of the British Caledonian Province. Lithos 105, 129–148.

Galer, S.J.G., 1997. Optimal triple spiking for high precision lead isotope ratio determination. Terra Nova Suppl. 9, 441.

Hässig, M., Rolland, Y., Sosson, M., Galoyan, G., Müller, C., Avagyan, A., Sahakyan, L., 2013. New structural and petrological data on the Amasia ophiolites (NW Sevan–Akera suture zone, Lesser Caucasus): insights for a large-scale obduction in Armenia and NE Turkey. Tectonophysics 588, 135–153.

Hirth, G., Kohlstedt, D., 1996. Water in the oceanic upper mantle: implications for rheology, melt extraction and the evolution of the lithosphere. Earth Planet. Sci. Lett. 144, 93–108.

Hirth, G., Kohlstedt, D., 2003. Rheology of the upper mantle and the mantle wedge: a view from the experimentalists. In: Eiler, J. (Ed.), Inside the Subduction Factory. American Geophysical Union Geophysical Monograph 183, pp. 83–105.

Ingle, S., Weis, D., Doucet, S., Mattielli, N., 2002. Hf isotope constraints on mantle sources and shallow-level contaminants during Kerguelen hot spot activity since ~120 Ma. Geochem. Geophys. Geosyst. 4, 1068. http://dx.doi.org/10.1029/2002GC000482.

Ionov, D.A., Bodinier, J.-L., Mukasa, S.B., Zanetti, A., 2002. Mechanisms and sources of mantle metasomatism: major and trace element compositions of peridotite xenoliths from Spitsbergen in the context of numerical modelling. J. Petrol. 43, 2219–2259.

Jackson, J., Haines, J., Holt, W., 1995. The accommodation of Arabia–Euasia Plate convergence in Iran. J. Geophys. Res. 100 (B8), P15205.

Jrbashian, R.T., Kazarian, G.A., Karapetian, S.G., Meliksetian, Kh.B., Mnatsakanian, A., Shirinian, K.G., 1996. Meso-Cenozoic basaltic volcanism in the northeastern part of Armenian Highland. Lett. Armenian Acad. Sci. Earth Sci. 49, 19–32 (in Russian).

Kaislaniemi, L., van Hunen, J., Allen, M.B., Neill, I., 2014. Sublithospheric small-scale convection — a mechanism for collision zone magmatism. Geology 42, 291–294.

Karakhanian, A., Vernant, P., Doerflinger, E., Avagyan, A., Philip, H., Aslanyan, R., Champollion, C., Arakelyan, S., Collard, P., Baghdasaryan, H., Peyret, M., Davtyan, V., Calais, E., Masson, F., 2013. GPS constraints on continental deformation in the Armenian region and Lesser Caucasus. Tectonophysics 92, 39–45.

Karapetian, S.G., Jrbashian, R.T., Mnatsakanian, A.Kh., 2001. Late collision rhyolitic volcanism in the north-eastern part of the Armenian Highland. J. Volcanol. Geotherm. Res. 112, 189–220.

Karapetyan, K.I., 1983. The Use of Archaeological Findings in Stratigraphic Subdivision of Volcanics in the Armenian Republic. Aspects of the Armenian Quaternary Geology, Yerevan, pp. 85–94 (No further details available).

Kay, R.W., Kay, S.M., 1993. Delamination and delamination magmatism. Tectonophysics 219, 177–189.

Kelemen, P.B., Hanghøj, K., Greene, A.R., 2003. One view of the geochemistry of subduction-related volcanic arcs, with an emphasis on primitive andesite and lower crust. In: Holland, H.D., Turkekian, H.H. (Eds.), Treatise on Geochemistry 3 "The Crust". Elsevier, Amsterdam, pp. 1–70.

Keskin, M., 2003. Magma generation by slab steepening and breakoff beneath a subduction-accretion complex: an alternative model for collision-related volcanism in Eastern Anatolia, Turkey. Geophys. Res. Lett. 30, 1–4.

Keskin, M., Can Genç, Ş., Tüysüz, O., 2008. Petrology and geochemistry of post-collisional Middle Eocene volcanic units in North-Central Turkey: evidence for magma generation by slab breakoff following the closure of the Northern Neotethys Ocean. Lithos 104, 267–305.

Kharazyan, E.Kh., 1983. Geology of Recent Volcanism of North-west Part of Armenian SSR (Basins of Rivers Dzoraget and Akhuryan). (Unpublished PhD thesis), ArmGeologia, Yerevan (55 pp.).

Kharazyan, E.Kh., 2005. Geological map of Armenia. Ministry of Nature Protection of Republic of Armenia (1 sheet).

Kharazyan, E.Kh., Shirinyan, K.G., 1981. Basaltic formation. Magmatic and Metamorphic Formations of Armenia, pp. 218–221 (in Russian; no further publication details available).

Kheirkhah, M., Allen, M.B., Emami, M., 2009. Quaternary syn-collision magmatism from the Iran/Turkey borderlands. J. Volcanol. Geotherm. Res. 182, 1–12.

Kheirkhah, M., Neill, I., Allen, M.B., Ajdari, K., 2013. Small-volume melts of lithospheric mantle during continental collision: Late Cenozoic lavas of Mahabad, NW Iran. J. Asian Earth Sci. 74, 37–49.

Kheirkhah, M., Neill, I., Allen, M.B., 2015. Petrogenesis of OIB-like basaltic volcanic rocks in a continental collision zone: Late Cenozoic magmatism of Eastern Iran. J. Asian Earth Sci. http://dx.doi.org/10.1016/j.jseaes.2015.02.027 (in press).

Koulakov, I., Zabelina, I., Amanatashvili, I., Meskhia, V., 2012. Nature of orogenesis and volcanism in the Caucasus region based on results of regional tomography. Solid Earth 3, 327–337.

Lambart, S., Laporte, D., Schiano, P., 2009. An experimental study of pyroxenite partial melts at 1 and 1.5 GPa: implications for the major element composition of Mid-Ocean Ridge Basalts. Earth Planet. Sci. Lett. 288, 335–347.

Le Bas, M.J., Le Maitre, R.W., Streckeisen, A., Zanettin, B., 1986. A chemical classification of volcanic rocks based on the total alkali–silica diagram. J. Petrol. 27, 745–750.

Lebedev, V.A., Bubnov, S.N., Dudauri, O.Z., Vashakidze, G.T., 2008a. Geochronology of Pliocene volcanism in the Dzhavakheti Highland (the Lesser Caucasus). Part 1: western part of the Dzhavakheti Highland. Stratigr. Geol. Correl. 16, 204–224.

Lebedev, V.A., Bubnov, S.N., Dudauri, O.Z., Vashakidze, G.T., 2008b. Geochronology of Pliocene volcanism in the Dzhavakheti Highland (the Lesser Caucasus). Part 2: eastern part of the Dzhavakheti Highland. Regional geological correlation. Stratigr. Geol. Correl. 16, 553–574.

Lebedev, V.A., Chernyshev, I.V., Yakushev, A.I., 2011. Initial time and duration of Quaternary magmatism in the Aragats neovolcanic area (Lesser Caucasus, Armenia). Dokl. Earth Sci. 437, 532–536.

Liotard, J.M., Dautria, J.M., Bosch, D., Condomines, M., Mehdizadeh, H., Ritz, J.F., 2008. Origin of the absarokite–banakite association of the Damavand volcano (Iran): trace elements and Sr, Nd, Pb isotope constraints. Int. J. Earth Sci. 97, 89–102.

Maggi, A., Priestley, K., 2005. Surface waveform tomography of the Turkish–Iranian plateau. Geophys. J. Int. 160, 1068–1080.

McCulloch, M.T., Gamble, J.A., 1991. Geochemical and geodynamic constraints on subduction zone magmatism. Earth Planet. Sci. Lett. 102, 358–374.

McDonough, W.F., Sun, S.-S., 1995. The composition of the Earth. Chem. Geol. 120, 223–253.

McQuarrie, N., van Hinsbergen, D.J.J., 2013. Retrodeforming the Arabia–Eurasia collision zone: age of collision versus magnitude of continental subduction. Geology 41, 315–318.

Mederer, J., Moritz, R., Ulianov, A., Chiaradia, M., 2013. Middle Jurassic to Cenozoic evolution of arc magmatism during Neotethys subduction and arc-continent collision in the Kapan Zone, southern Armenia. Lithos 177, 61–78.

Meliksetian, Kh., 2013. Pliocene–Quaternary volcanism of the Syunik upland. Veröffentlichungen des Landesamtes für Denkmalpflege und Archäologie Sachsen-Anhalt pp. 247–258.

Mirnejad, H., Hassanzadeh, J., Cousens, B.L., Taylor, B.E., 2010. Geochemical evidence for deep mantle melting and lithospheric de-lamination as the origin of the inland Damavand volcanic rocks of northern Iran. J. Volcanol. Geotherm. Res. 198, 288–296.

Missenard, Y., Cadoux, A., 2012. Can Moroccan Atlas lithospheric thinning and volcanism be induced by Edge-Driven Convection? Terra Nova 24, 27–33.

Mitchell, J., Westaway, R., 1999. Chronology of Neogene and Quaternary uplift and magmatism in the Caucasus: constraints from K–Ar dating of volcanism in Armenia. Tectonophysics 304, 157–186.

Miyashiro, A., 1978. Nature of alkalic volcanic rock series. Contrib. Mineral. Petrol. 66, 91–104.

Morley, C.K., Kongwung, B., Julapour, A.A., Abdolghafourian, M., Hajian, M., Waples, D., Warren, J., Otterdoom, H., Srisuriyon, K., Kazemi, H., 2009. Structural development of a major late Cenozoic basin and transpressional belt in central Iran: the Central Basin in the Qom-Saveh area. Geosphere 5, 325–362.

Mumladze, T., Forte, A.M., Cowgill, E.S., Trexler, C.C., Niemi, N.A., Yikilmaz, M.B., Kellogg, L.H., 2015. Subducted, detached, and torn slabs beneath the Greater Caucasus. GeoResJ 5, 36–46.

Münker, C., Pfänder, J.A., Weyer, S., Büchl, A., Kleine, T., Mezger, K., 2003. Evolution of Planetary Cores and the Earth/Moon System from Nb/Ta Systematics. Science 301, 84–87.

Neill, I., Meliksetian, Kh., Allen, M.B., Navarsardyan, G., Karapetyan, S., 2013. Pliocene–Quaternary volcanic rocks of NW Armenia: magmatism and lithospheric dynamics within an active orogenic plateau. Lithos 180–181, 200–215.

Nikogosian, I., Meliksetian, Kh., van Bergen, M., Mason, P., Jrbashyan, R., Navasardyan, G., Ghukasyan, Y., Melkonyan, R., Karapetyan, S., 2014. Characteristics of mantle sources in Jurassic to Quaternary magmatic history of the territory of Armenia, as a guide to diverse geodynamic settings. Geophys. Res. Abstr. 16, EGU2014–EGU2262.

Niu, Y., Hékinian, R., 1997. Spreading rate-dependence of the extent of mantle melting beneath mid-ocean ridges. Nature 385, 326–329.

Niu, Y., Zhao, Z., Zhu, D.-C., Mo, X., 2013. Continental collision zones are primary sites for net continental crust growth. Earth Sci. Rev. 127, 96–110.

Nowell, G.M., Kempton, P.D., Noble, S.R., Fitton, J.G., Saunders, A.D., Mahoney, J.J., Taylor, R.N., 1998. High precision Hf isotope measurements of MORB and OIB by thermal ionisation mass spectrometry: insights into the depleted mantle. Chem. Geol. 149, 211–233.

Ottley, C.J., Pearson, D.G., Irvine, G.J., 2003. A routine method for the dissolution of geological samples for the analysis of REE and trace elements via ICP-MS. In: Holland, J.G., Tanner, S.D. (Eds.), Plasma Source Mass Spectrometry: Applications and Emerging Technologies. Royal Society of Chemistry, Cambridge, pp. 221–230.

Özdemir, Y., Güleç, N., 2014. Geological and geochemical evolution of the Quaternary Süphan stratovolcano, Eastern Anatolia, Turkey: evidence for the lithosphere–asthenosphere interaction in post-collision volcanism. J. Petrol. 55, 37–52.

Özdemir, Y., Karaoğlu, Ö., Tolluoğlu, A.Ü., Güleç, N., 2006. Volcanostratigraphy and petrogenesis of the Nemrut stratovolcano (East Anatolian High Plateau): the most recent post-collisional volcanism in Turkey. Chem. Geol. 226, 189–211.

Pang, K.-N., Chung, S.-L., Zarrinkoub, M.H., Lin, Y.-C., Lee, H.-Y., Lo, C.-H., Khatib, M.M., 2013. Iranian ultrapotassic volcanism at ~11 Ma signifies the initiation of post-collision magmatism in the Arabia–Eurasia collision zone. Terra Nova 25, 405–413.

Pearce, J.A., 1983. Role of the sub-continental lithosphere in magma genesis at active continental margins. In: Hawkesworth, C.J., Norry, M.J. (Eds.), Continental Basalts and Mantle Xenoliths. Shiva, Natwich, pp. 230–249.

Pearce, J.A., Bender, J.F., Delong, S.E., Kidd, W.S.F., Low, P.J., Guner, Y., Sargolu, F., Yilmaz, Y., Moorbath, S., Mitchell, J.G., 1990. Genesis of collision volcanism in eastern Anatolia, Turkey. J. Volcanol. Geoth. Res. 44, 189–229.

Peccerillo, R., Taylor, S.R., 1976. Geochemistry of Eocene calc-alkaline volcanic rocks from the Kastamonu area, northern Turkey. Contrib. Mineral. Petrol. 58, 63–81.

Pertermann, M., Hirschmann, M.M., 2003. Partial melting experiments on a MORB-like pyroxenite between 2 and 3 GPa: constraints on the presence of pyroxenite in basalt source regions from solidus location and melting rate. J. Geophys. Res. 8 (B2), 2125. http://dx.doi.org/10.1029/2000JB000118.

Piromallo, C., Morelli, A., 2003. P-wave tomography of the mantle under the Alpine–Mediterranean area. J. Geophys. Res. 108, B2. http://dx.doi.org/10.1029/2002JB001757.

Plank, T., 2005. Constraints from thorium/lanthanum on sediment recycling at subduction zones and the evolution of the continents. J. Petrol. 46, 921–944.

Presnall, D.C., Gudfinnsson, G.H., Walter, M.J., 2002. Generation of mid-ocean ridge basalts at pressures from 1 to 7 GPa. Geochim. Cosmochim. Acta 66, 2073–2090.

Presnyakov, S.L., Belyaeva, E.V., Lyubin, V.P., Rodionov, N.V., Antonov, A.V., Saltykova, A.K., Berezhnaya, N.G., Sergeev, S.A., 2012. Age of the earliest Paleolithic sites in the northern part of the Armenian Highland by SHRIMP-II U–Pb geochronology of zircons from volcanic ashes. Gondwana Res. 21, 929–938.

Priestley, K., McKenzie, D., Barron, J., Tatar, M., Debayle, E., 2012. The Zagros core: deformation of the continental lithospheric mantle. Geochem. Geophys. Geosyst. 13. http://dx.doi.org/10.1029/2012GC004435.

Robinson, J.A.C., Wood, B.J., 1998. The depth of the spinel to garnet transition at the peridotite solidus. Earth Planet. Sci. Lett. 164, 277–284.

Rolland, Y., Billo, S., Corsini, M., Sosson, M., Galoyan, G., 2009. Blueschists of the Amassia–Stepanavan suture zone (Armenia): linking Tethys subduction history from E-Turkey to W-Iran. Int. J. Earth Sci. 98, 533–550.

Rolland, Y., Sosson, M., Adamia, S., Sadradze, N., 2011. Prolonged Variscan to Alpine history of an active Eurasian margin (Georgia, Armenia) revealed by ^{40}Ar/^{39}Ar dating. Gondwana Res. 20, 798–815.

Rolland, Y., Perincek, D., Kaymacki, N., Sosson, M., Barrier, E., Avagyan, A., 2012. Evidence for ~80–75 Ma subduction jump during Anatolide–Tauride–Armenian block accretion and ~48 Ma Arabia–Eurasia collision in Lesser Caucasus–East Anatolia. J. Geodyn. 56–57, 76–85.

Rollinson, H.R., 1993. Using Geochemical Data. Routledge (384 pp.).

Rooney, T.O., Nelson, W.R., Dosso, L., Furman, T., Hanan, B., 2014. The role of continental lithosphere metasomes in the production of HIMU-like magmatism on the northeast African and Arabian plates. Geology 42, 419–422.

Rosman, K.J.R., Taylor, P.D.P., 1998. Isotopic compositions of the elements 1997. Pure Appl. Chem. 70, 217–235.

Rudnick, R.L., Gao, S., 2003. Composition of the continental crust. In: Holland, H.D., Turekian, H.H. (Eds.), Treatise on Geochemistry 3 "The Crust". Elsevier, Amsterdam, pp. 1–56.

Saal, A.E., Hart, S.R., Shimizu, N., Hauri, E.H., Layne, G.D., Eiler, J.M., 2005. Pb isotopic variability in melt inclusions from the EMI–EMII–HIMU mantle end-members and the role of the oceanic lithosphere. Earth Planet. Sci. Lett. 240, 605–620.

Şengör, A.M.C., 1984. The Cimmeride orogenic system and the tectonics of Eurasia. Geol. Soc. Am. Spec. Pap. 195, 1–74.

Şengör, A.M.C., 1990. A new model for the late Palaeozoic–Mesozoic tectonic evolution of Iran and implications for Oman. In: Robertson, A.H.P., Searle, M.P., Ries, A.C. (Eds.), The Geology and Tectonics of the Oman Region. Geological Society of London Special Publications 49, pp. 797–831.

Şengör, A.M.C., Natal'in, B.A., 1996. Turkic-type orogeny and its role in the making of the continental crust. Annu. Rev. Earth Planet. Sci. 24, 263–337.

Şengör, A.M.C., Okuroğullari, A.H., 1991. The role of accretionary wedges in the growth of continents: Asiatic examples from Argand to plate tectonics. Eclogae Geol. Helv. 84, 535–597.

Şengör, A.M.C., Özeren, M.S., Keskin, M., Sakın ç, M., Özbak r, A.D., Kayan, I., 2008. Eastern Turkish high plateau as a small Turkic-type orogen: implications for post-collisional crust-forming processes in Turkic-type orogens. Earth-Sci. Rev. 90, 1–48.

Shaw, D.M., 2005. Trace Elements in Magmas, a Theoretical Treatment. Cambridge University Press, Cambridge (243 pp.).

Sheth, H., Meliksetian, Kh., Gevorgyan, H., Israyelyan, A., Navasardyan, G., 2015. Intracanyon basalt lavas of the Debed River (northern Armenia), part of a Pliocene-Pleistocene continental flood basalt province in the South Caucasus. Journal of Volcanology and Geothermal Research 295, 1–15.

Shirtladze, N.I., 1958. Post Paleogene Effusive Volcanism of Georgia Tiblisi, 335 pp (No further details available).

Sizova, E., Gerya, T., Brown, M., 2014. Contrasting styles of Phanerozoic and Precambrian continental collision. Gondwana Res. 25, 522–545.

Skolbeltsyn, G., Mellors, R., Gök, R., Türkelli, N., Yetirmishli, G., Sandvol, E., 2014. Upper mantle S wave velocity structure of the East Anatolian–Caucasus region. Tectonics 33, 207–221.

Sosson, M., Rolland, Y., Müller, C., Danelian, T., Melkonyan, R., Kekelia, S., Adamia, A., Babazadeh, V., Kangarli, T., Avagyan, A., Galoyan, G., Mosar, J., 2010. Subductions, obduction and collision in the Lesser Caucasus (Armenia, Azerbaijan, Georgia), new insights. In: Sosson, M., Kaymakci, N., Stephenson, R.A., Bergerat, F., Starostenko, V. (Eds.), Sedimentary Basin Tectonics from the Black Sea and Caucasus to the Arabian Platform. Geological Society of London Special Publications 340, pp. 329–352.

Stampfli, G.M., 2000. Tethyan oceans. In: Bozkurt, E., Winchester, J.A., Piper, J.D.A. (Eds.), Tectonics and Magmatism in Turkey and the Surrounding Area. Geological Society of London Special Publications 173, pp. 1–23.

Steiger, R.H., Jager, E., 1977. Subcommission on geochronology: convention on the use of decay constants in geo- and cosmochronology. Earth Planet. Sci. Lett. 36, 359–362.

Sun, S.-S., McDonough, W.F., 1989. Chemical and isotopic systematics of oceanic basalts: implications for mantle composition and processes. In: Saunders, A.D., Norry, M.J. (Eds.), Magmatism in the Ocean Basins. Geological Society of London Special Publication vol.42, pp. 313–345.

Turner, S., Sandiford, M., Foden, J., 1992. Some geodynamic and compositional constraints on 'postorogenic' magmatism. Geology 20, 931–934.

van Hunen, J., Allen, M.B., 2011. Continental collision and slab break-off: a comparison of 3-D numerical models with observations. Earth Planet. Sci. Lett. 302, 27–37.

Verdel, C., Wernicke, B.P., Hassanzadeh, J., Guest, B., 2011. A Paleogene extensional arc flare-up in Iran. Tectonics 30. http://dx.doi.org/10.1029/2010TC002809 (TC3008).

Vernant, P., Nilforoushan, F., Hatzfeld, D., Abbassi, M., Vigny, C., Masson, F., Nankali, H., Martinod, J., Ashtiani, A., Bayer, R., Tavakoli, F., Chery, J., 2004. Contemporary crustal deformation and plate kinematics in Middle East constrained by GPS measurements in Iran and northern Iran. Geophys. J. Int. 157, 381–398.

Walter, M.J., 1998. Melting of garnet peridotite and the origin of komatiite and depleted lithosphere. J. Petrol. 39, 26–60.

Wieser, M.E., 2006. Atomic weights of the elements 2005. Pure Appl. Chem. 78, 2051–2066.

Williams, H.M., Turner, S.P., Pearce, J.A., Kelley, S.P., Harris, N.B.W., 2004. Nature of the source regions for post-collisional potassic magmatism in southern and northern Tibet from geochemical variations and inverse trace element modelling. J. Petrol. 45, 555–607.

Workman, R.K., Hart, S.R., 2005. Major and trace element composition of the depleted MORB mantle (DMM). Earth Planet. Sci. Lett. 231, 53–72.

Wu, F.-Y., Sun, D.-Y., Li, H., Jahn, B.-M., Wilde, S., 2002. A-type granites in northeastern China: age and geochemical constraints on their petrogenesis. Chem. Geol. 187, 143–173.

Zhao, Z.-F., Dai, L.-Q., Zheng, J.-F., 2013. Postcollisional mafic igneous rocks record crust-mantle interaction during continental deep subduction. Nat. Sci. Rep. 3. http://dx.doi.org/10.1038/srep03413.

Zor, E., 2008. Tomographic evidence of slab detachment beneath eastern Turkey and the Caucasus. Geophys. J. Int. 175, 1273–1282.